Consortium

for

Small-Scale Modelling

Technical Report No. 27

The COSMO Priority Project 'COLOBOC': Final Report

July 2015

DOI: 10.5676/DWD_pub/nwv/cosmo-tr_27

Deutscher Wetterdienst
MeteoSwiss
Ufficio Generale Spazio Aereo e Meteorologia
ΕΘΝΙΚΗ ΜΕΤΕΩΡΟΛΟΓΙΚΗ ΥΠΗΡΕΣΙΑ
Instytucie Meteorogii i Gospodarki Wodnej
Administratia Nationala de Meteorologie
ROSHYDROMET
Agenzia Regionale per la Protezione Ambientale del Piemonte
Agenzia Regionale per la Protezione Ambientale dell'Emilia-Romagna
Centro Italiano Ricerche Aerospaziali
Amt für GeoInformationswesen der Bundeswehr

www.cosmo-model.org

Editor: Massimo Milelli, ARPA Piemonte

The COSMO Priority Project 'COLOBOC': Final Report

Project participants:

J-M. Bettems[*], *H. Asensio*, *G. Bonafe*, *G. Duniec*, *O. Fuhrer*, *J. Helmert*, *C. Heret*, *E. Kazakova*, *M. Lange*, *E. Machulskaya*, *A. Mazur*, *G. de Morsier*, *G. Rianna*, *I. Rozinkina*, *B. Vieli*, *G. Vogel*

[*] Project coordinator:
Jean Marie Bettems
MeteoSchweiz
Kundendienst
OperationCenter 1
Postfach 257
CH-8058 Zürich-Flughafen
Switzerland

1 Introduction

Atmospheric processes such as the development of the boundary layer, low level cloudiness, and the onset and intensity of convection are significantly influenced by the evolution of the lower boundary conditions. Consequently, an accurate representation of exchange processes between the soil and the atmosphere is essential to produce high quality NWP forecasts. At the time of the definition of the project, many activities concerning the lower boundary of the COSMO model had been undertaken, but most of these activities lacked some final efforts to bring them into operations and to make them accessible to the whole COSMO community. In 2008, the COSMO steering committee (STC) established a new Priority Project named Consolidation of Lower Boundary Conditions (COLOBOC), to finalize these developments and to incorporate them into well tested and documented software packages. The project was structured in 8 tasks, namely:

- Facilitate the access and usage of soil and surface observations (task 0)
- Consolidate an externalized TERRA module (task 1)
- Consolidate the software used to generate the external parameters (task 2)
- Consolidate and extend the external parameters database (task 3)
- Find and validate an optimal configuration of TERRA with its associated external parameters and look-up tables (task 4)
- Revise the snow model and the snow analysis (task 5)
- Deploy an urban module developed at EPFL/Switzerland (task 6)
- Consolidate the parameterization of land surface heterogeneity (task 7)

The project spanned the period 09.2008 to 09.2011; during these 3 years, about 8.5 FTE have been invested, with resources coming from 6 different institutions. Many discussions with colleagues of the CLM community took place during this project, resulting in the organization of regular COSMO / CLM meeting around this topic. Although not all tasks were successful (see chapter 3 for details), most of the developments done during this project have resulted in follow-up activities in the COSMO working group dedicated to soil and surface activities (see http://www.cosmo-model.org/content/tasks/workGroups/wg3b/default.htm).

2 State of the modelling system at the start of the project

The soil vegetation atmosphere transfer (SVAT) scheme TERRA and the associated external parameters provide the terrestrial lower boundary conditions for the atmospheric component of the COSMO model. TERRA is a multilayer model with a direct solution of the heat conduction equation and considers moisture transport due to hydraulic processes within the soil and the effects of transpiration by plants. Phase change processes of soil water (freezing/thawing of soil water/ice) are incorporated in the scheme both for their thermodynamic effect and for their impact on the hydraulic properties of the soil. In addition, the COSMO model employs a single layer snow module considering melting of a snow pack with prognostic snow density and time dependent snow albedo. Many uncertainties in the description and simulation of surface characteristics are partly caused by well-known problems. A critical

issue is the limited knowledge of the physical properties of the surface in the form of the so-called external parameters (e.g. soil type, root depth). These parameters play a vital role, e.g. in the simulation of the hydrological state, but both the quality of the raw databases and the methods used to derive the required model properties from these databases are not optimal. Moreover, the increase in horizontal resolution of current NWP models implies that some surface types previously neglected, such as lake and urban regions, are becoming more important. The simulation of the evolution of the soil is also hampered by inadequate knowledge of the initial state. Unrealistic drifts in soil moisture are ubiquitous in most NWP models, due to both incorrect representation of soil processes and the accumulation of precipitation errors (Scipal and Drusch, 2007). As demonstrated for the global model GME, an improvement may be achieved through a change in the root density distribution together with the introduction of seasonal vegetation parameters (Ritter, 2007). Due to the non-linear relations between surface parameters and fluxes, neglecting subgrid-scale land-surface heterogeneities by using average external parameters, may result in erroneous flux estimates. Studies have shown that, even with a grid spacing of only a few kilometres, considerable aggregation effects may indeed occur and must be corrected for. This can be tackled by introducing one of the so-called tile or mosaic approaches: the surface within a coarse scale atmospheric grid box is subdivided into patches with assumed homogeneous surface characteristics, fluxes are computed for each patch separately and then averaged. The current representation of the snow does not allow liquid water to stay within the snow pack, which is a severe limitation in spring when the freezing of trapped water during the night slows down the melting of the snow pack. Furthermore, many local effects such as snow transport by wind and influence of slope orientation make a correct representation of the snow cover particularly difficult.

3 Tasks and achievements

A summary of the different project tasks and of the achieved results are presented in this chapter. More details on some of these developments can be found in the following chapters.

Task 0: Facilitate the access and usage of soil and surface observations.

Goals: convenient access to recent operational high quality observations, representative for different climate and different type of soils.

Achievements: an action started in October 2009 with an official letter sent to a selection of NMS directors. Soil and surface data from 9 European observatories is now available on-line, in a common ASCII format (see http://www.cosmo-model.org/srnwp/content/default.htm). Time series starts in 2006; recent data is added each year, with 6 months time lag. The DWD has agreed to support this action in the future (C.Heret, F.Beyrich). This action is also supported by the C-SRNWP Programme of EUMETNET.

Open issues: only 5 sites are regularly updated (Cabauw, Lindenberg, Payerne, SP Capofiume, Sodankyla). Users community is small.

Task 1: Consolidate an externalized TERRA module.

TERRA standalone is the isolated terrestrial surface module of COSMO driven by external atmospheric fields, taken either from observations or from model runs. This tool provides a computationally efficient way to generate balanced soil conditions for the whole integration domain by computing multi-years TERRA integrations; it is also a useful tool to experiment with the soil model and the external parameters. It has been originally developed by F. Ament.

Goals: clean-up and consolidate the TERRA standalone code.

Achievements: a consolidated package, based on COSMO release 4.13, including documentation, is available on the COSMO web site (see http://www.cosmo-model.org/content/support/software/default.htm).

Open issues: the code is not compliant with the COSMO standard. The TERRA standalone code is not integrated in the COSMO software, making the synchronization with the model development difficult. No COSMO resource is available to further support this code, in particular to coordinate multiple developments taking place in the CLM community (the situation has changed at the time of writing of this report, IMS being interested taking over this duty).

Task 2: Consolidate the software used to generate the external parameters for the COSMO model.

Goals: the software infrastructure should be flexible and modular in order to support various raw datasets and to allow for experimentation with new aggregation algorithms or different look-up tables. It should be easily extensible to support future external parameters. It should support the needs of COSMO, COSMO-CLM, ICON, and GME.

Achievements: a software, called EXTPAR, fulfilling the stated goals and well documented, has been developed (see the Extpar user and implementation manual at http://www.cosmo-model.org/content/model/modules). At the time of writing of this report, this software is an official COSMO software, kept on a centralized repository at CSCS, with D. Lüthi as source code administrator; EXTPAR can now be activated through a web interface hosted on the CLM web site (http://www.clm-community.eu/index.php?menuid=221).

Open issues: none.

Task 3: Consolidate and extend the external parameters database.

Goals: a survey of external parameter fields and raw data sources used within the COSMO and the COSMO-CLM community will be performed. Where appropriate, replace older data sets by newer ones. Adapt work done for the GME. Consolidate external parameters required for new extensions of TERRA.

Achievements: the databases used for the external parameters have been updated according to the stated goals (see http://www.cosmo-model.org/content/model/modules/externalParams/default.htm).

In particular, a total of 15 new external parameters have been added: (vegetation characteristics) NDVI, NDVI_MX, NDVI_RATIO, RSMIN, (surface characteristics) EMISS_RAD, (deep soil) T2M_CL, (topo corrected radiation) SLOPE_ASP, SLOPE_ANG, HORIZON, SKYVIEW, (urban fraction) URBAN, (lake model) FR_LAKE, DEPTH_LK, (aerosols) AER_BC, AER_DUST, AER_SO4, AER_SS.

Open issues: the need to update the external parameters will always be present, e.g. for higher resolution applications or when new parameters are required for newly developed model parameterizations.

Task 4: Find and validate an optimal configuration of TERRA with its associated external parameters and look-up tables.

Goals: (1) gather and integrate tested developments of TERRA in official COSMO code, (2) define a consolidated set of look-up tables, (3) find and validate an optimal reference configuration of TERRA, using the external parameters and the consolidated look-up tables

developed within task 3.

Achievements: many experiments have been done to evaluate the impact of improved parameterizations, new external parameters and updated look-up tables. A new unified consolidated configuration, based on COSMO release 4.11, used both for the global scale in GME and for the regional scale in COSMO, has been defined. Experiments at MeteoSwiss and at DWD with this consolidated configuration showed mixed, neutral impact on verification scores; however, this consolidated configuration provides a physically sound basis for further developments. More details are available in chapter 4 of this report.

Open issues: compensating errors in different parts of the model hinders the development of TERRA.

Task 5: Revise the snow model and the snow analysis.

Goals: (1) Finalize and deploy a new multi-layer snow model supporting change of phases within the snow pack, (2) combine and improve a snow analysis approach based on in-situ observations and MSG derived snow mask.

Achievements: a detailed analysis of the performance of COSMO-RU has shown very large T2m errors in spring, up to 12 deg, at the boundary of the snow pack; these errors could be related to inadequate values of the snow water equivalent provided by the global snow analysis cycle. Different approaches have been proposed by our Russian colleagues to circumvent this issue (new parameterization of the snow density, observation driven 1D snow model). The work on the snow model has resulted in a revised parameterization of the snow albedo (incl. ageing), in a revised parameterization of the partial snow cover (height instead of snow water equivalent based), and in an experimental implementation of the multi-layers snow model in release 4.11 of COSMO (see chapter 5 for a description of this new snow model). The snow analysis software used at DWD (sfcana) has been adapted to support the use of the MSG derived snow mask.

Open issues: the multi-layers snow model has still some stability issues, in particular for very shallow snow layers, and needs more testing (at the time of writing of this report, the development of the multi-layers snow model has been transferred in ICON but is still not finalized). More generally, snow analysis and modelling still requires more work, in particular in complex terrain, during the snow melting period, or when going to finer resolution.

Task 6: Deploy an urban module developed at EPFL/Switzerland.

Goals: Consolidate and transfer an urban model developed at EPFL/Switzerland, based on the Buildings Effects Parametrization (BEP), into the latest COSMO release.

Achievements: an implementation of BEP, including some documentation, is available in a COSMO private release at MeteoSwiss (based on COSMO release 4.7). The description of the BEP implementation in COSMO, and of its impact, is available in chapter 6 of this report.

Open issues: no code responsible has been found. Furthermore, due to the complexity of this urban model, possibly not suited for general NWP applications, the decision to take it in the official COSMO release is pending (at the time of writing of this report, the choice of a simpler urban parameterization for the official COSMO release has been made).

Task 7: Consolidate the parameterization of land surface heterogeneity.

Goals: Finalize and deploy an implementation of the tile/mosaic approach, using the developments of Ament, 2006, implemented in a COSMO private release at MeteoSwiss.

Achievements: these developments have been consolidated and transferred in COSMO release 4.16. Dynamic snow tile has been introduced. Sensitivity studies have been performed, without conclusive results about the impact of this parameterization.

Open issues: code implementation is still experimental and has not been validated by COSMO Source Code Administrator (at the time of writing of this report, the COLOBOC implementation has been discarded and a new tile parameterization has been fully re-implemented in the ICON model).

4 Experiments towards an unified soil-vegetation atmosphere transfer scheme TERRA for global and limited-area numerical weather prediction (J. Helmert, G. Vogel, H. Asensio, J. M. Bettems, M. Lange, F. Brenner, B. Ritter)

4.1 Introduction

One of the critical issues in the description and simulation of surface characteristics in atmospheric models is due to physical surface properties in the form of the so-called external parameters (e.g. soil type, vegetation state, root depth, plant physiological parameters). These parameters play a crucial role, e.g. in the simulation of the hydrological state, but both, the variable quality of the raw databases and the used methods to retrieve the required model properties from these databases contribute to uncertainties in NWP model forecasts.

Together with the external parameters the soil vegetation atmosphere transfer (SVAT) scheme TERRA provides the terrestrial lower boundary conditions for the atmospheric component of the global GME model and the limited-area COSMO model. Driven by radiation fluxes, the evolution of the lower boundary conditions influence the exchange of heat, moisture, and momentum between the surface and the atmosphere and has a large impact on the simulation of screen level variables and atmospheric processes, such as the development of the boundary layer, low level cloudiness, and the onset and intensity of convection.

The SVAT model TERRA is a multilayer model with a direct solution of the heat conduction equation and considers moisture transport due to hydraulic processes within the soil and the effects of transpiration by plants. Phase change processes of soil water (freezing/thawing of soil water/ice) are incorporated in the scheme both for their thermodynamic effect and for their impact on the hydraulic properties of the soil. A snow module (single or multilayer) is employed considering melting of a snow pack with prognostic snow density and time dependent snow albedo. However, there is a need to employ also a canopy layer for vegetation in TERRA to improve the surface energy budget in COSMO.

Although the global GME and the limited-are COSMO model share the SVAT model TERRA in large parts it is reasonable to test new developments first on the global scale. Therefore a number of changes in external parameters and modifications of TERRA are used in operational GME, that are still experimental in COSMO. To fill this gap in the SVAT model between GME and COSMO a unified configuration for TERRA that further improves the lower boundary condition of NWP models at global and regional scale is proposed. For soil moisture analysis (SMA), employed to minimize the difference between diagnosed 2m-temperature and observations this unification between COSMO and GME is now achieved (Lange, 2011).

The report starts with the operational and experimental configuration of GME and COSMO-EU, both models with SMA, then show a case study at 10th April 2011 to illustrate the sensitivity of the results on the applied configuration. Long-term simulations of GME and COSMO-EU are evaluated from soil-moisture analyis monitoring and objective verification followed by a summary and an outlook. The appendix contains figures that refers to changes in external parameters.

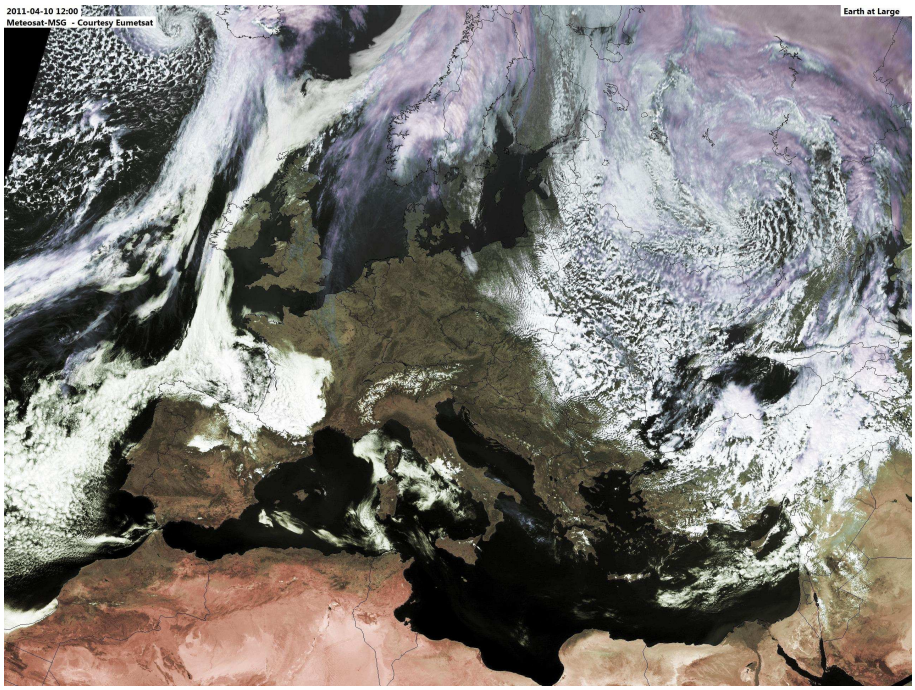

Figure 1: Meteosat VIS image of Europe on 10th April 2011 12 UTC

4.2 Model configuration

The differences in model configuration with impact on the energy budget at surface between GME and COSMO include the aerosol distribution, surface emissivity, vegetation albedo, vegetation climatology, root density profile, and minimum stomatal resistance (Tab. 1).

The radiation budget at Earth surface forces the energy fluxes into the atmosphere and to the ground. The magnitude of these fluxes depends on the amount of incoming global radiation, which is altered primarily by clouds and aerosols. While the global model GME uses a aerosol climatology from Tegen et al. (1997), the COSMO model employs a constant distribution of aerosols according to Tanre et al. (1984) with a known overestimation of desert dust aerosol in Europe (e.g. Hohenegger et al., 2005). In order to obtain a similar surface radiation budget in COSMO in comparison with GME, the aerosol climatology from Tegen et al. (1997) was applied in the COSMO experiment that used similar to the GME the land-use dependent surface emissivity.

In addition to the incoming radiation, the surface radiation budget of vegetation covered areas depends also on the vegetation albedo. The approach of a constant vegetation albedo of 15 % is enhanced in the numerical experiments of GME and COSMO, following e.g. Moody et al. (2008) by taking into account the land-use by distinction of evergreen (10 %), deciduous (15 %) , and non-forest (20 %). Given the radiation budget at surface, the partition of energy fluxes is influenced by the evapotranspiration depending on plant physiological parameters. The prescribed annual cycle of vegetation parameters (e.g leaf-area index (LAI) and vegetation fraction) in the outer-tropics depending on latitude and height (Doms et al., 2005) was modified in the GME and the COSMO experiments by employing an annual cycle from the climatology (1998-2003) of the normalized differential vegetation index (NDVI).

The partition of energy fluxes at the surface depends also on a large extent on the soil moisture (Balsamo et al., 2009), that has therefore a large impact on the Bowen ratio.

	GME	COSMO-EU	GME EXP	COSMO-EU EXP
Model status	operational	operational	109/1009	8474
Aerosol distribution	climatology	fixed	climatology	climatology
Emissivity	land-use	const	land-use	land-use
Vegetation albedo	const	const	land-use	land-use
Vegetation climatology	NDVI	analytical	NDVI	NDVI
Root density profile	exponential	uniform	exponential	exponential
Min. stomatal resistance	GLC2000	const	ECOCLIMAP	ECOCLIMAP

Table 1: Configuration of GME and COSMO routine and numerical experiments.

However, the simulation of the evolution of the soil is hampered by inadequate knowledge of the initial state. Unrealistic drifts in soil moisture are ubiquitous in most NWP models, due to both incorrect representation of soil processes and the accumulation of precipitation errors (Scipal and Drusch, 2008). As already demonstrated for the global model GME, an improvement may be achieved through the introduction of the NDVI-based annual cycle of vegetation together with a change in the root density distribution (Ritter, 2007). The exponential root density profile used in GME was employed also in the COSMO model and applied in the limited-area experiments.

The maximum possible evapotranspiration of plants is connected with a minimum stomatal resistance r_{min}. The constant value of this parameter of 150 $sm^{-}1$ in the COSMO model was replaced by a land-use dependent formulation from GME. However it was found in GME that large uncertainties in the value of r_{min} for individual land-use classes exist that leads to a domain averaged overestimation of r_{min}. In connection with the soil-moisture analysis (SMA) that was adapted from COSMO to the GME to minimize the difference between diagnosed 2m-temperature and observations (Lange, 2011), an overestimation of r_{min} results in an accumulation of soil moisture. To further improve the SMA in GME and COSMO the relationship between land-use classes and r_{min} was adapted from ECOCLIMAP Masson et al. (2003) and applied in numerical experiments of GME and COSMO. From the observed reduction of domain averaged r_{min}, a more realistic annual cycle of soil moisture with reduced SMA increments was expected.

4.3 Numerical experiments - Case study 10th April 2011

The soil-moisture analysis was introduced in the operational GME at 9th March 2011 for the 00 UTC analysis. The accompanying numerical GME experiment (experiment code 109/1009) was initialized at 12th March 2011 00 UTC, which applies the land-use based vegetation albedo and minimal stomatal resistance from land-use classes of ECOCLIMAP. In order to allow for a spin-up of the GME experiment the numerical COSMO experiment (experiment code 8474) was initialized at 1st April 2011 00 UTC. This spin-up is considered as sufficient for atmospheric processes and processes of the upper soil. It used the boundary conditions from 109/1009 and shares the configuration of the external parameters and the SVAT scheme with the global model experiment.

As a case study the sensitivity of the COSMO-EU 36 hour forecast on the used configuration was investigated for a clear-sky situation in central Europe on the 10th April 2011 12 UTC. Figure 1 shows the visible satellite image on this date with a large cloud-free area in central

Europe.

As shown in Tab. 1, the GME experiment 109/1009 uses the same configuration setup as the COSMO experiment 8474. Therefore, the following figures show the absolute values for the GME experiment and the difference between operational COSMO-EU and the COSMO experiment 8474 assuming a much smaller difference between GME experiment 109/1009 and the COSMO experiment 8474. The 36 hour forecast of the averaged net radiation budget at surface from the GME experiment (Fig. 2 top) shows small values in North-Scandinavia due to the snow pack with high albedo compared to the snow free regions in central Europe. The difference of the averaged net radiation budget at surface between operational COSMO-EU and COSMO-EU experiment 8474 reveals the changes in aerosol optical depth, vegetation albedo, and surface emissivity. The dominant effect of the reduced desert dust aerosol optical depth leads to the expected increase of the averaged net radiation budget at surface in the domain mean.

The surface albedo (Fig. 14 top) is dominated by snow in northern Europe and the mountains but the difference in the snow free regions refers to the changes in annual cycle of vegetation and formulation of the vegetation albedo (Fig. 14, bottom). The modified albedo of evergreen forest (set to 10 % in the experiment) is visible for the low-mountain range of central Europe. An additional contribution to the difference in vegetation albedo comes from the vegetation coverage (Fig. 15, top). Replacing the analytical function by a NDVI-based climatology leads to a significant higher vegetation coverage in south-west and central Europe and a decrease north-east after the first third of April (Fig. 15, bottom) .

As expected this is also the case for the leaf ara index LAI (Fig. 16). The GME experiment (Fig. 16, top) refers the LAI to the NDVI climatology and shows therefore realistic maximum values in south-western Europe. The comparison to the operational COSMO-EU (Fig. 16, bottom) shows that the difference to the empirical relationship in this region is increased.

For the plant evapotranspiration, in addition to the LAI, the minimum stomatal resistance r_{min} is one important vegetation parameter (Fig. 17, top) . The impact of the relationship of the land-use classes to r_{min} based on ECOCLIMAP is large, exceeding 30 sm^{-1} in domain average (Fig. 17, bottom). Only for the low-mountain range and Scandinavia the difference is below 15 sm^{-1}.

In the average over the forecast time, a sensitivity of the heat fluxes on the differences in external parameters and SVAT model is expected. Figure 3 (top) shows the averaged sensible heat flux (positive downward) those difference for COSMO is a result of changes in surface radiation budget (Fig. 2) and differences in partition of energy at the surface. Positive values of the sensible heat flux averaged over forecast time reveals the cooling over the snow (Fig. 3, top) but the mean value over the domain increased by about 8 Wm^{-2} for the COSMO-EU experiment that is larger than the increase in averaged latent heat flux (Fig. 4) of below 4 Wm^{-2}. However, even regions in western and central Europe and northern Africa with different vegetation properties (higher vegetation coverage, LAI, smaller minimum stomatal resistance, different root density profile) in the COSMO-EU experiment compared to the operational COSMO-EU exceeds this value clearly. Considering the change in the Bowen ratio based on sensible and latent heat flux averaged over the forecast time, Fig. 5 supports this result since regions in western Europe with positive Bowen ratio below one, i.e. less sensitive heat flux than latent heat flux with same sign, show a positive difference to the operational COSMO-EU. It could be expected that the increased latent heat flux in the COSMO-EU experiment is correlated with a decrease in soil moisture and Fig. 6 confirms this assumption. Due to the exponential root density profile in the experiment the impact of the upper soil levels on the evapotranspiration is increased that leads to 10 % dryer upper soil in parts of western Europe and northern Africa (Fig. 6, top). Here, the correlation of

this pattern to the changes in vegetation parameters is obvious. The modified root water uptake leads as expected to a soil moisture increase in the soil layers 54 cm and 162 cm (Fig. 6, center). However due to the large time scales in the deeper soil after 10 days of the numerical experiment the change in this case study is just small and below 5 %. This is also the case for considering all six hydraulic active layers in TERRA (Fig. 6, bottom), where the soil moisture increase for the experiment in domain average is 0.15 %.

Although feedback effects of changes in the SVAT scheme on precipitation could be assumed, their identification within one case study is difficult. This is confirmed by considering the accumulated precipitation fractions over 36 hours forecast time (Fig. 7). In this situation the increase in domain average is 0.05 kgm^{-2} for grid-scale and for convective precipitation with a small increase of the convective fraction on total precipitation in the COSMO-EU experiment.

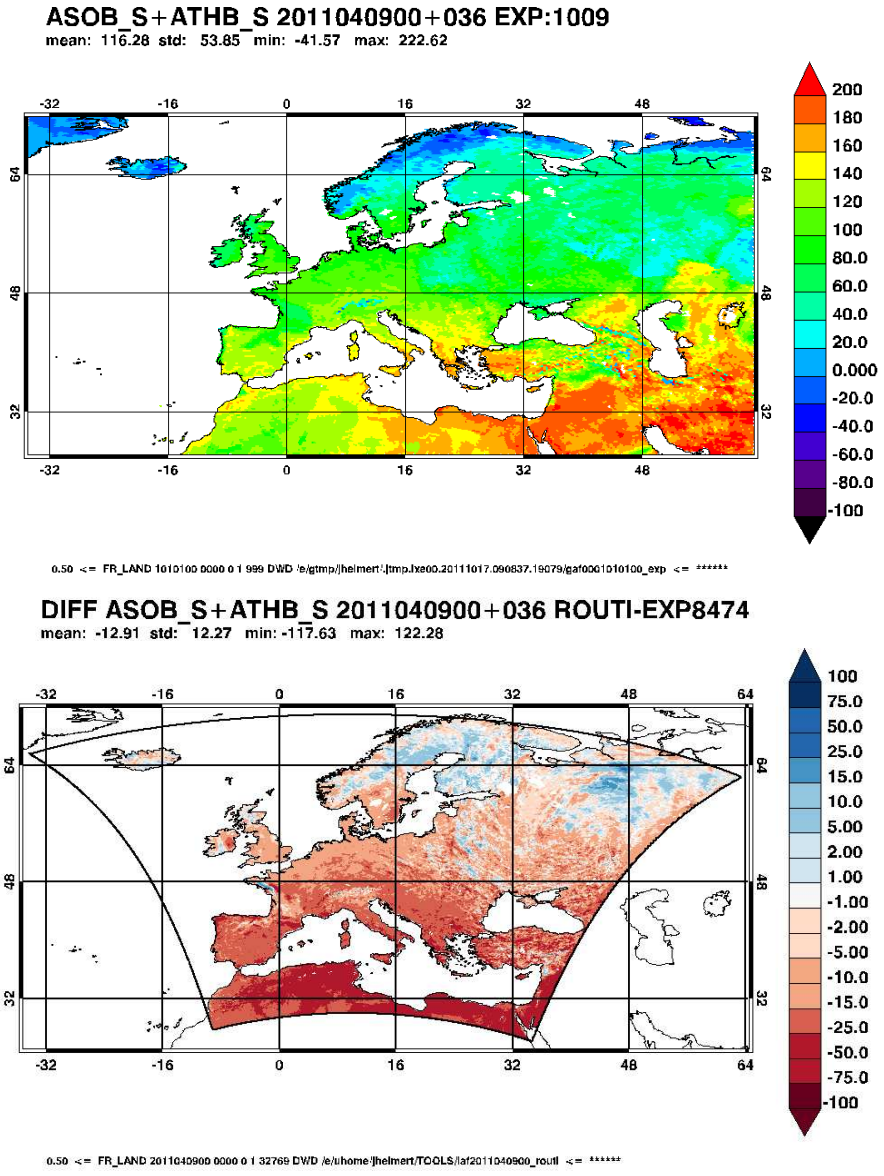

Figure 2: Averaged fluxes of solar and thermal radiation at surface (W/m^{-2}) at 10th April 2011 12 UTC for 36 hours forecast of the GME experiment 109/1009 (top) and difference between COSMO-EU routine and experiment 8474 (bottom)

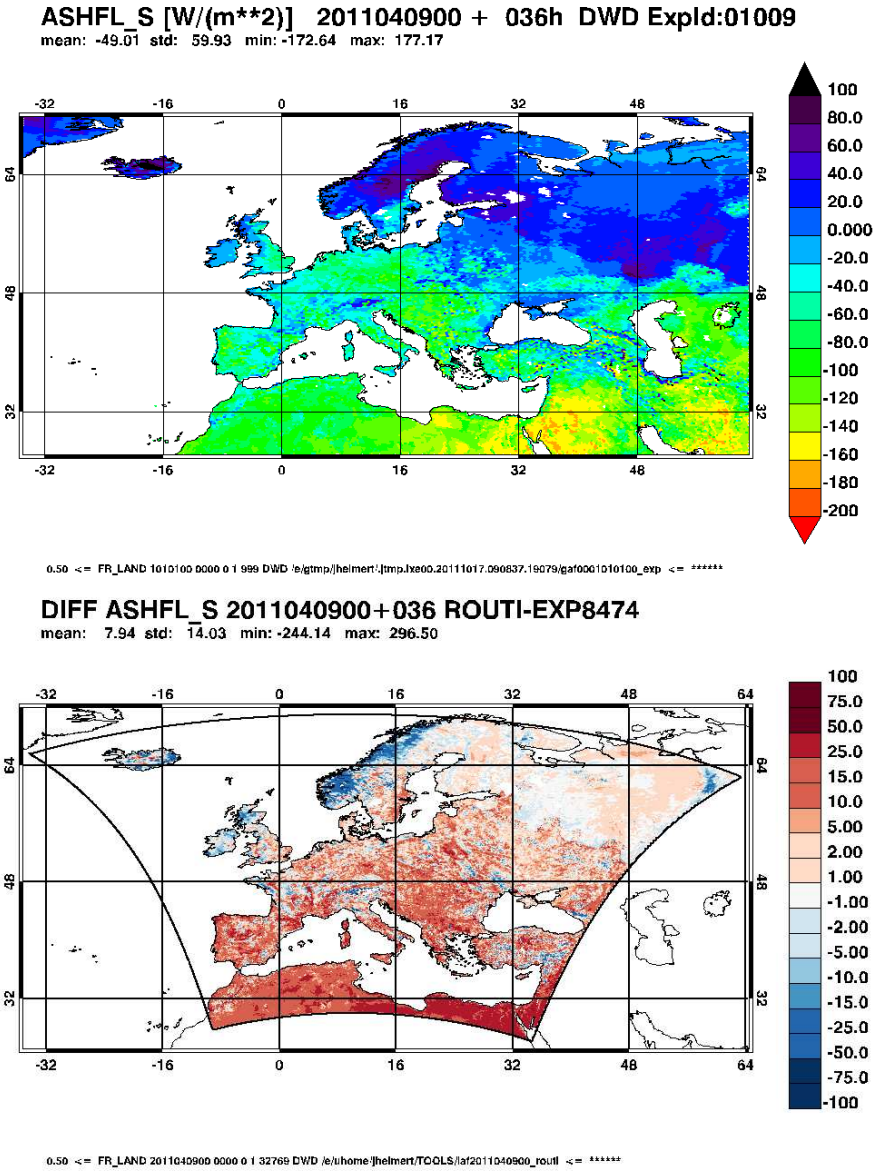

Figure 3: Flux of sensible heat (Wm^{-2}) averaged over 36 hours forecast time at 10th April 2011 12 UTC of the GME experiment 109/1009 (top) and difference between COSMO-EU routine and experiment 8474 (bottom).

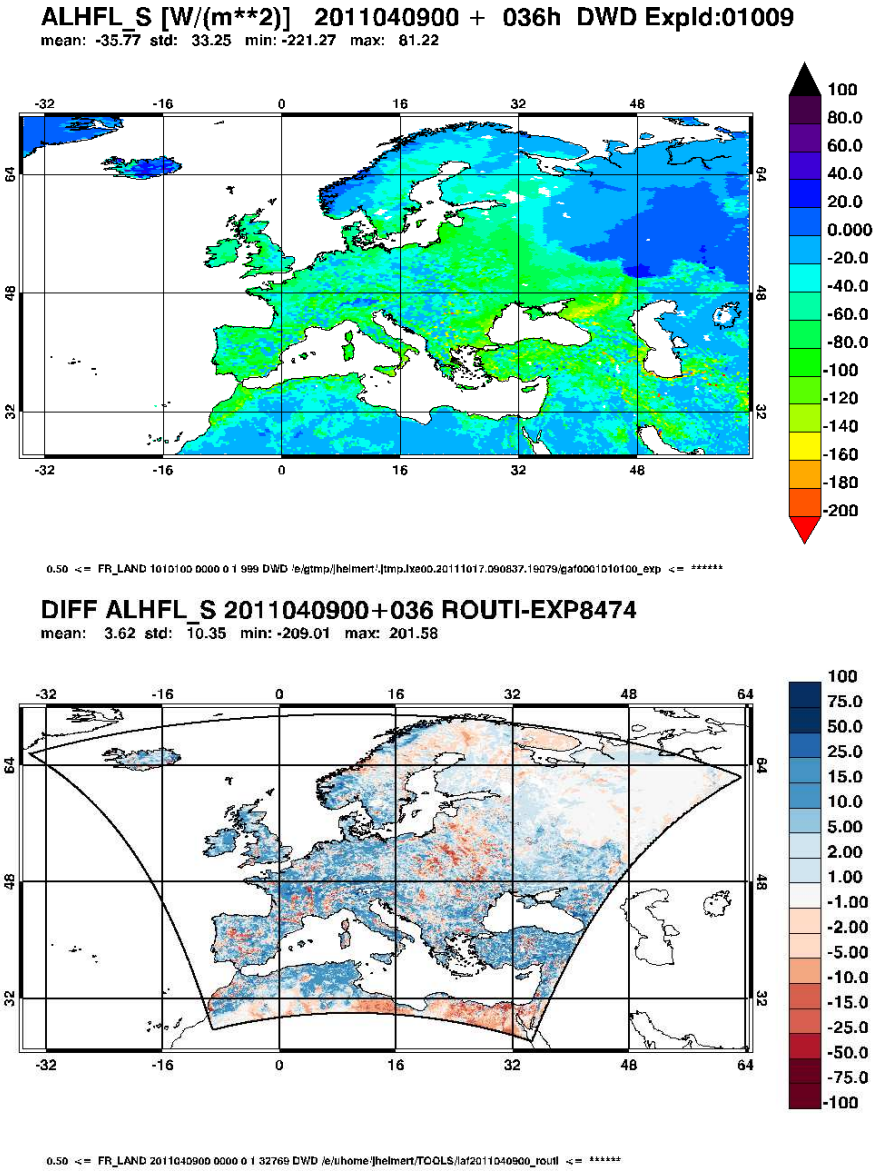

Figure 4: Flux of latent heat (Wm^{-2}) averaged over 36 hours forecast time at 10th April 2011 12 UTC of the GME experiment 109/1009 (top) and difference between COSMO-EU routine and experiment 8474 (bottom).

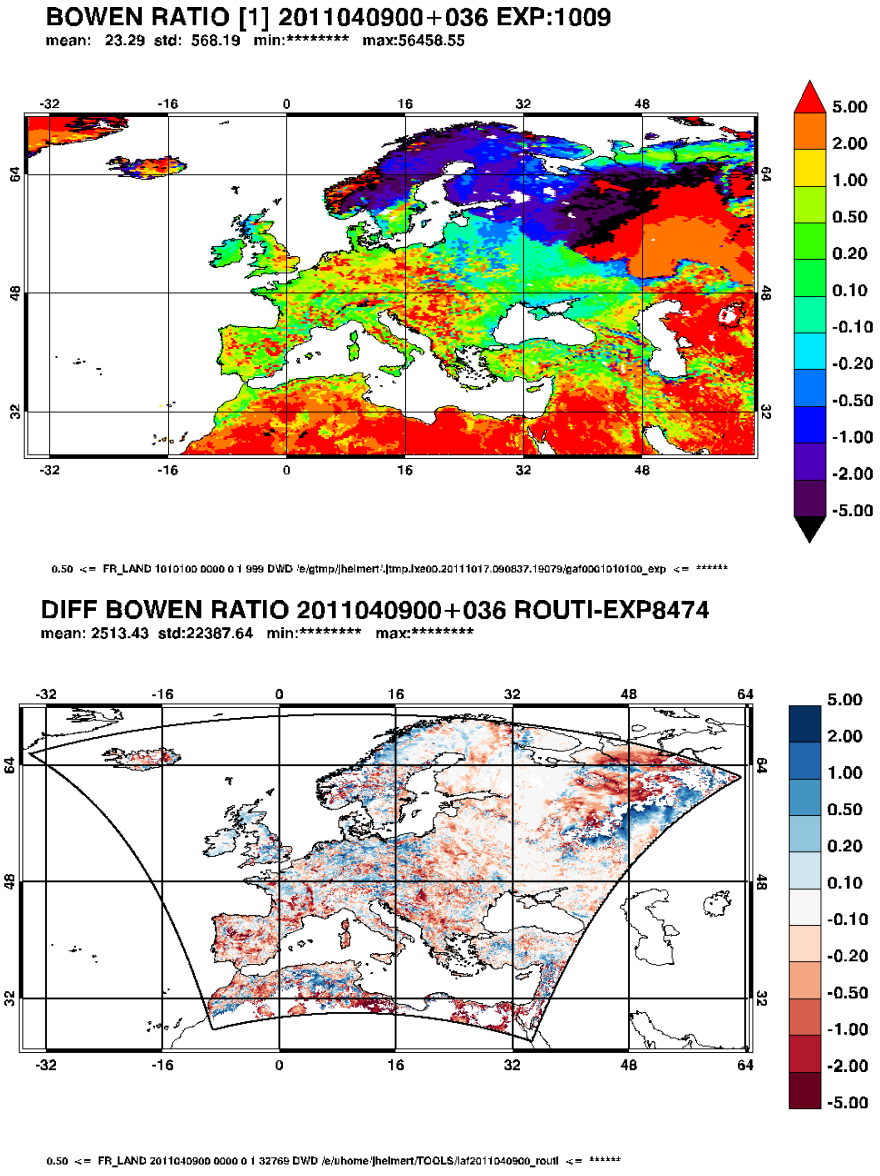

Figure 5: Bowen ratio based on flux of sensible and latent heat averaged over 36 hours forecast time at 10th April 2011 12 UTC of the GME experiment 109/1009 (top) and difference between COSMO-EU routine and experiment 8474 (bottom).

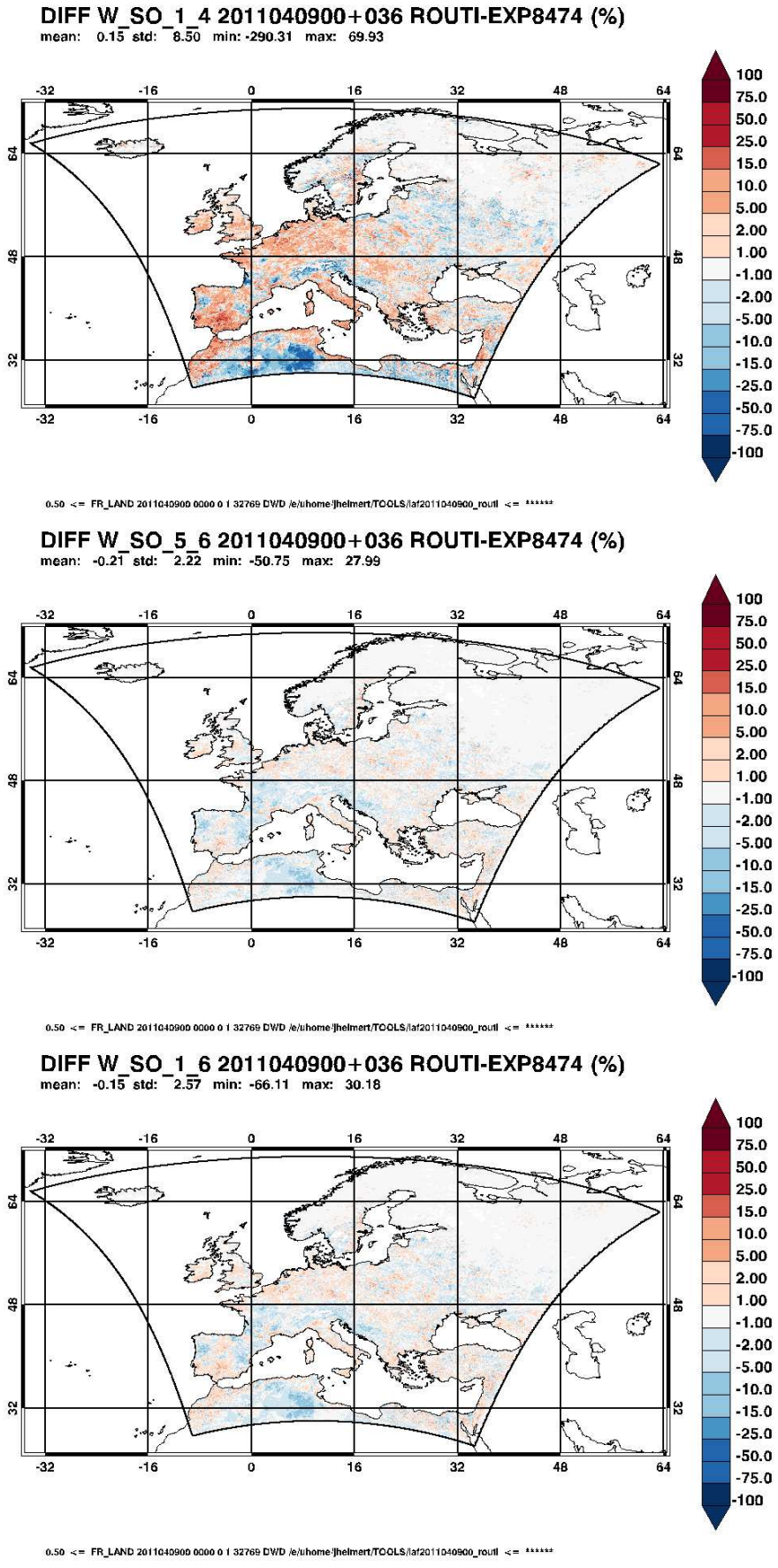

Figure 6: Difference between COSMO-EU routine and experiment 8474 for soil moisture including upper soil levels 1,2,6,18 cm (a), deeper soil levels 54 cm and 162 cm (b), and soil levels 1,2,6,18,54, and 162 cm (c). Shown is the deviation (%) in comparison to the COSMO-EU routine.

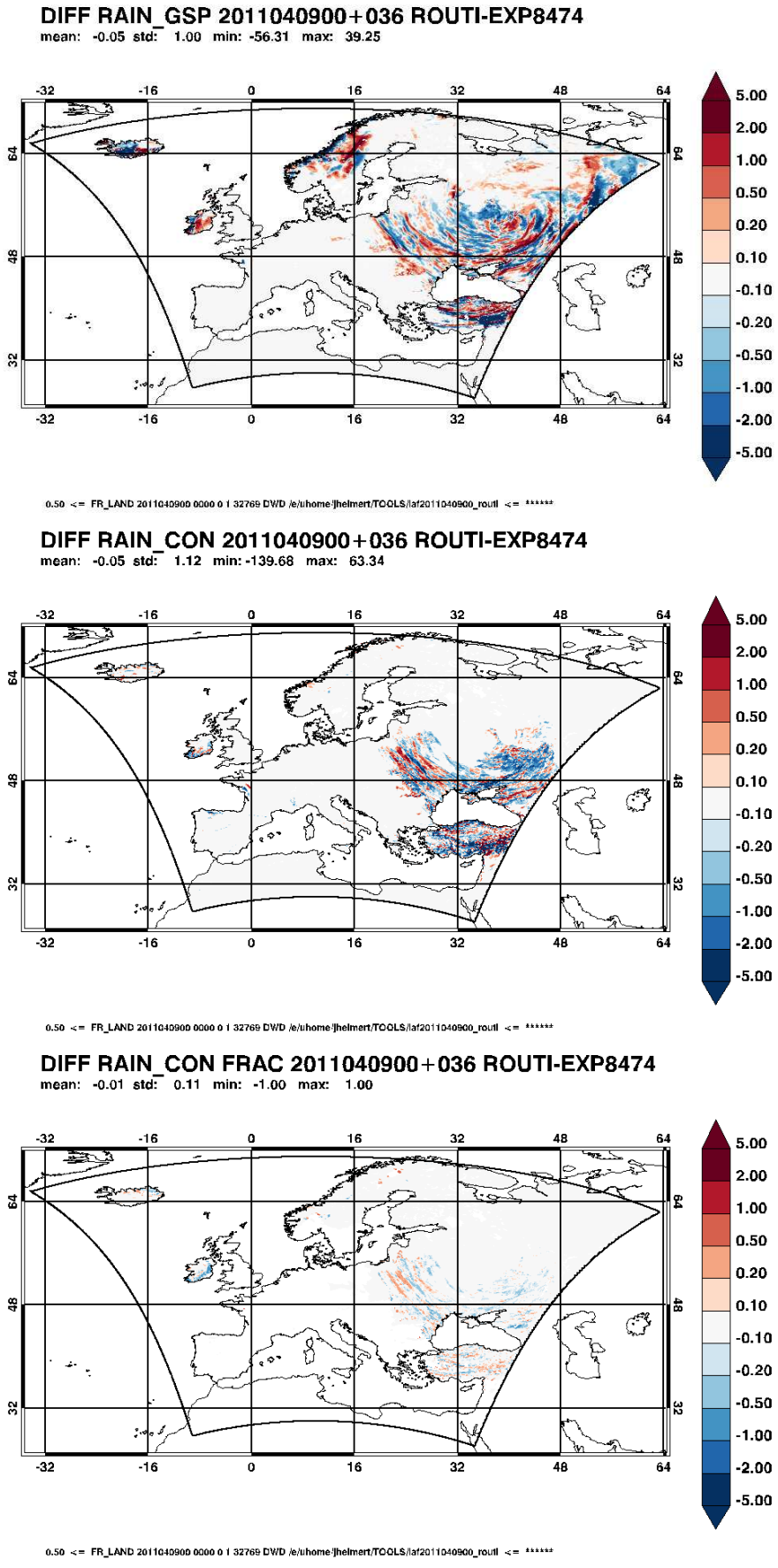

Figure 7: Difference between COSMO-EU routine and experiment 8474 for accumulated precipitation (kgm^{-2}) of grid-scale component (top), convective component (center), and fraction of convective component on total precipitation (grid-scale + convective) (bottom).

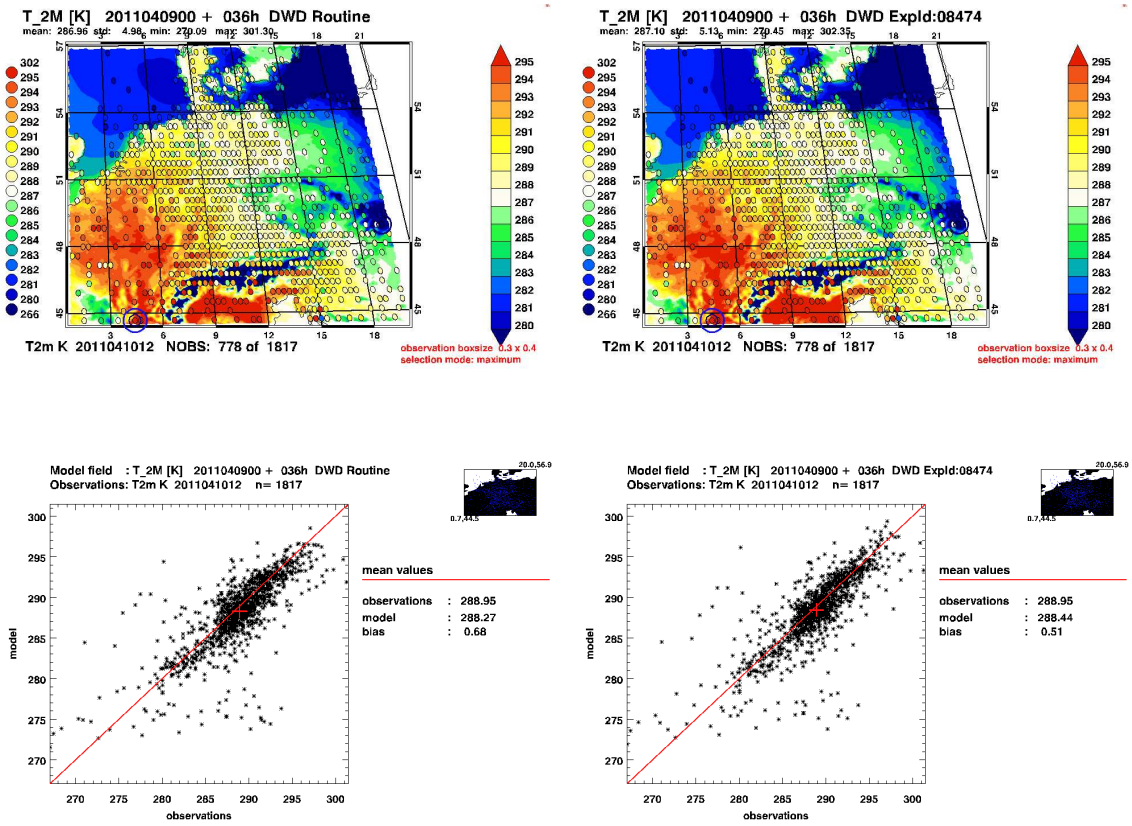

Figure 8: Comparison of 2m-temperature observations at 2011041012 and 36 hours forecast from 2011040900 of COSMO-EU routine (a) and experiment 8474 (b).

To exclude the impact of different cloud conditions in observation and model simulation, the clear sky region in central Europe was used for a validation of the COSMO-EU results with measurements at SYNOP stations. Figure 8 (top) shows that the difference in 2 m-temperature between operational COSMO and COSMO experiment is small, below 0.2 K in the area mean, but some measurements in northern Italy and France are in better agreement with the experiment. The statistical analysis (Fig. 8, bottom) confirms that considering 1817 observations the cold bias of 2 m-temperature of 0.68 K in the operational COSMO decreased in the experiment by 0.17 K that is mainly due to a better representation of 2 m-temperatures above 290 K in the experiment. This behaviour can be related to the impact of the aerosol climatology from Tegen et al. (1997).

Due to the changes in external parameters and in the SVAT scheme a feedback on the 2 m-dew point temperature can be assumed. Figure 9 (top) reveals that in area mean the difference in 2 m-dew point temperature of more than 0.4 K between operational COSMO-EU and experiment exceeds the difference in 2 m-temperature and by eye a better agreement with observations in the western region of the selected area can be found. For the 1869 observations the operational COSMO model bias of 2 m-dew point temperature was decreased from 3.10 K by 0.86 K in the experiment. The comparison of the model field with observations (Fig. 9, bottom) shows that a better capture of 2 m-dew point temperature in the range of 270 K to 280 K in the experiment is responsible for this improvement.

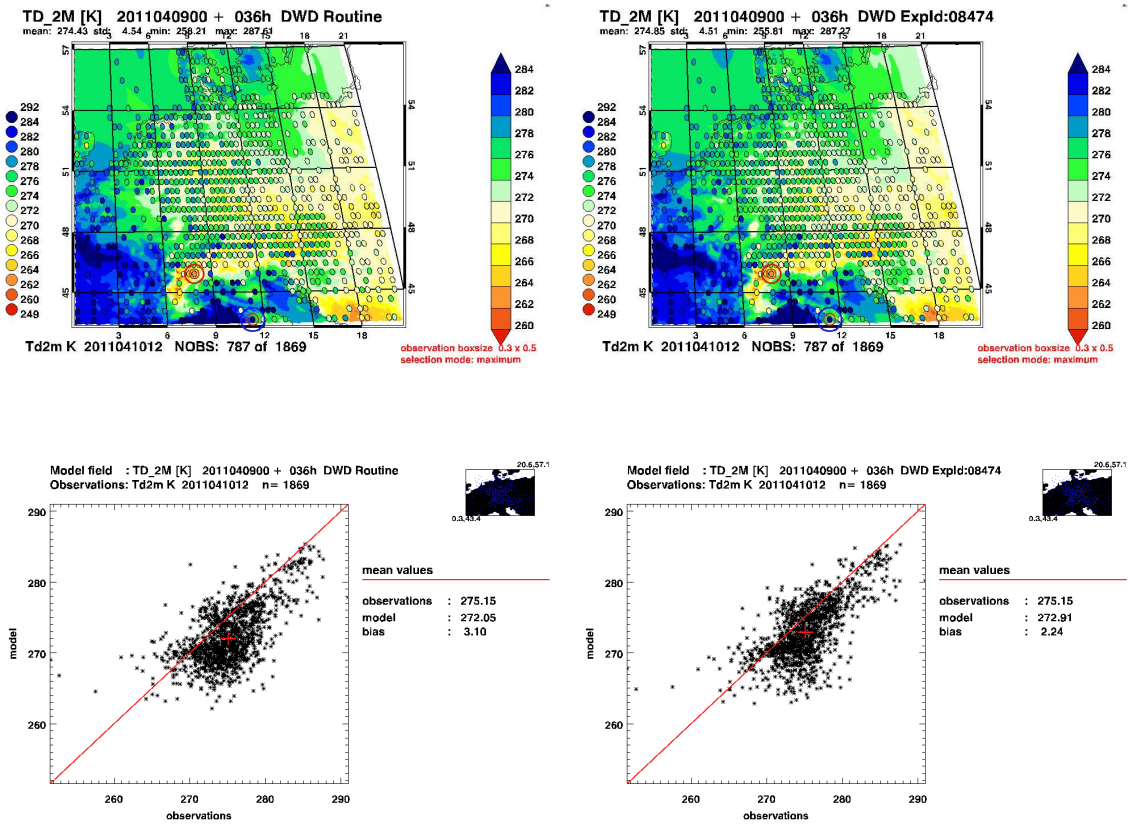

Figure 9: Comparison of 2m-dew point temperature observations at 2011041012 and 36 hours forecast from 2011040900 of COSMO-EU routine (a) and experiment 8474 (b).

4.4 Long-term results

A long-term comparison of the behavior of TERRA in the operational setup and with the new configuration in the soil-moisture analysis environment is available for the global model GME. Based on 24 hours forecasts Fig. 10 shows that the 2 m-temperature bias of GME in Europe (operational and experiment) changes its sign during April to the warm side for summer. Whereas the GME experiment 109/1009 shows similar RMSE values of 2 m-temperature as the operational simulations, the temperature bias in summer, when evapotranspiration of plants is most active in Europe is significantly reduced. Since the SMA diminishes their activity for the experiment by reduced soil water increments in top and bottom SMA layers it could be assumed that this is due to a more realistic behavior of TERRA in the experimental configuration. This assumption is further supported by the comparison of the soil moisture evolution in operational GME and experiment. The unrealistic nearly constant soil moisture in bottom SMA layer is improved by the experiment, which shows a decrease of soil moisture during summer that is confirmed by observations.

For the COSMO simulations an objective verification of the forecasts up to 72 hours against SYNOP stations in the COSMO-EU domain between 1st April 2011 and 30th June 2011 (Fig. 11 and 12) shows as expected largest changes in model bias of 2 m-temperature (TT) and 2 m-dew point temperature difference (TD) and surface pressure (P). However, verification shows a mixed picture. The bias and RMSE of 2 m-temperature and 2 m-dew point temperature difference increased but for surface pressure and 2-m minimum temperature (Tmin) an improvement was observed. In the global skill the experimental setup of COSMO-EU increased by 0.55 % compared to the operational setup.

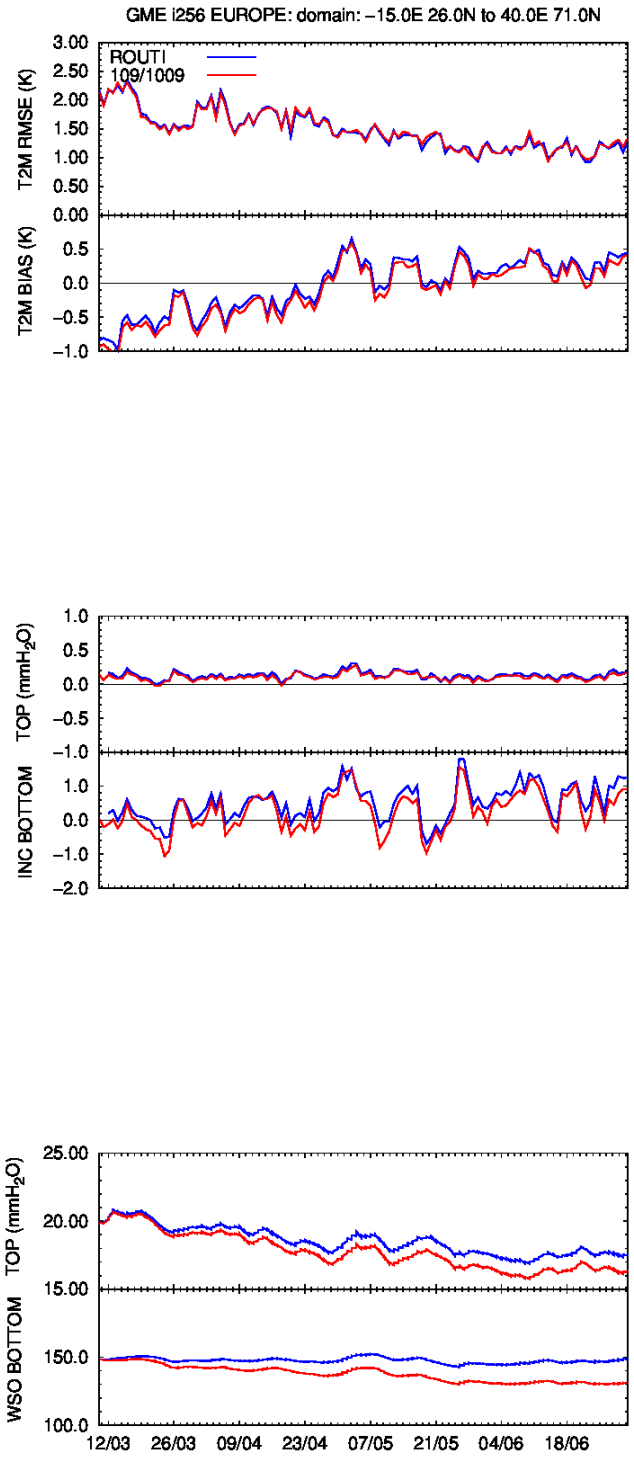

Figure 10: Comparison of operational GME (blue) and GME experiment 109/1009 (red) from soil-moisture analysis monitoring for Europe between 12th March 2011 and 1st July 2011. Shown are RMSE and bias of 2 m temperature (top), soil moisture analysis increments in top and bottom layers (center), and soil moisture evolution for top and bottom layers (bottom).

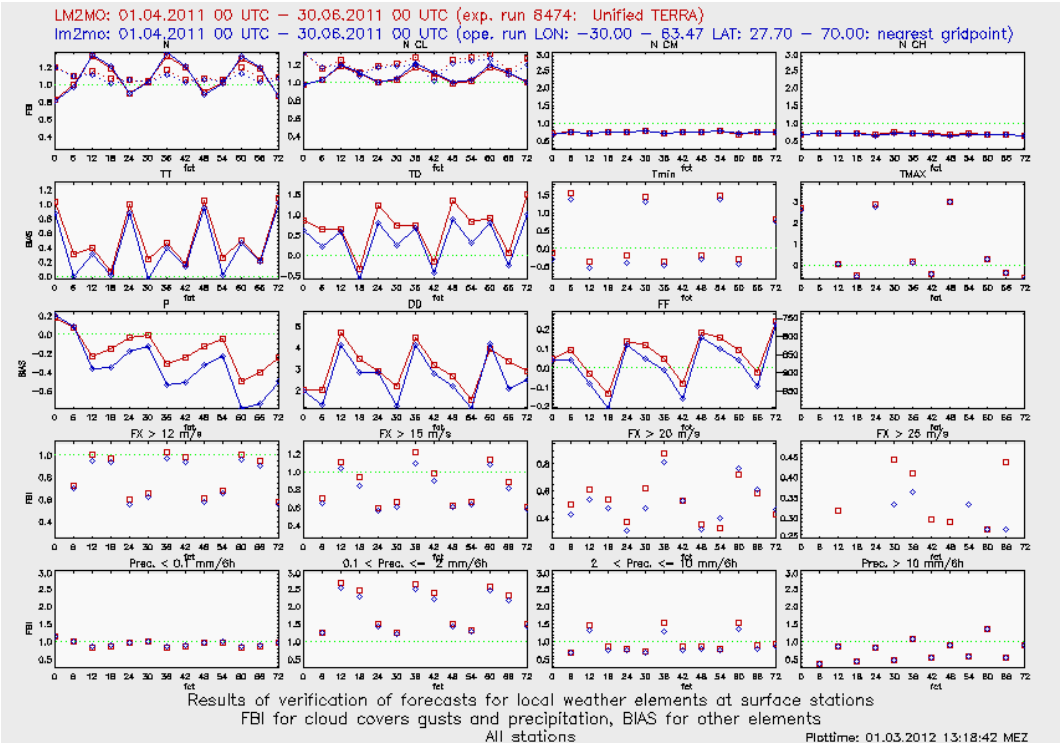

Figure 11: Objective verification up to 72 hours forecast between 1st April 2011 00 UTC and 30th June 2011 00 UTC in the model domain of operational COSMO-EU (blue) and numerical experiment 8474 (red). The verification is based on 00 UTC forecasts and considers FBI of cloud coverage (top row), bias of 2 m-temperature, 2 m-dew point temperature, minimum and maximum temperature (second row), surface pressure, wind direction, wind speed, and vector wind (center row), FBI for wind gusts of different threshold (fourth row), FBI for precipitation of different threshold (bottom row).

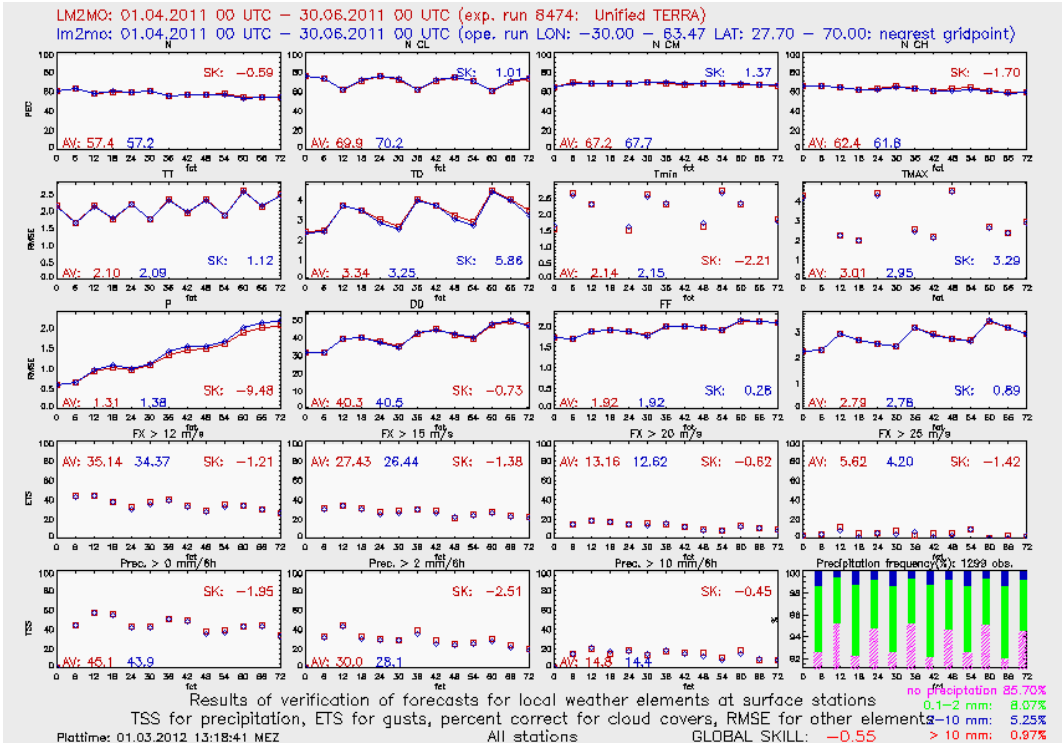

Figure 12: Objective verification up to 72 hours forecast between 1st April 2011 00 UTC and 30th June 2011 00 UTC in the model domain of operational COSMO-EU (blue) and numerical experiment 8474 (red). The verification is based on 00 UTC forecasts and considers PEC of cloud coverage (top row), RMSE of 2 m-temperature, 2 m-dew point temperature, minimum and maximum temperature (second row), surface pressure, wind direction, wind speed, and vector wind (center row), ETS for wind gusts of different threshold (fourth row), ETS for precipitation of different threshold (bottom row).

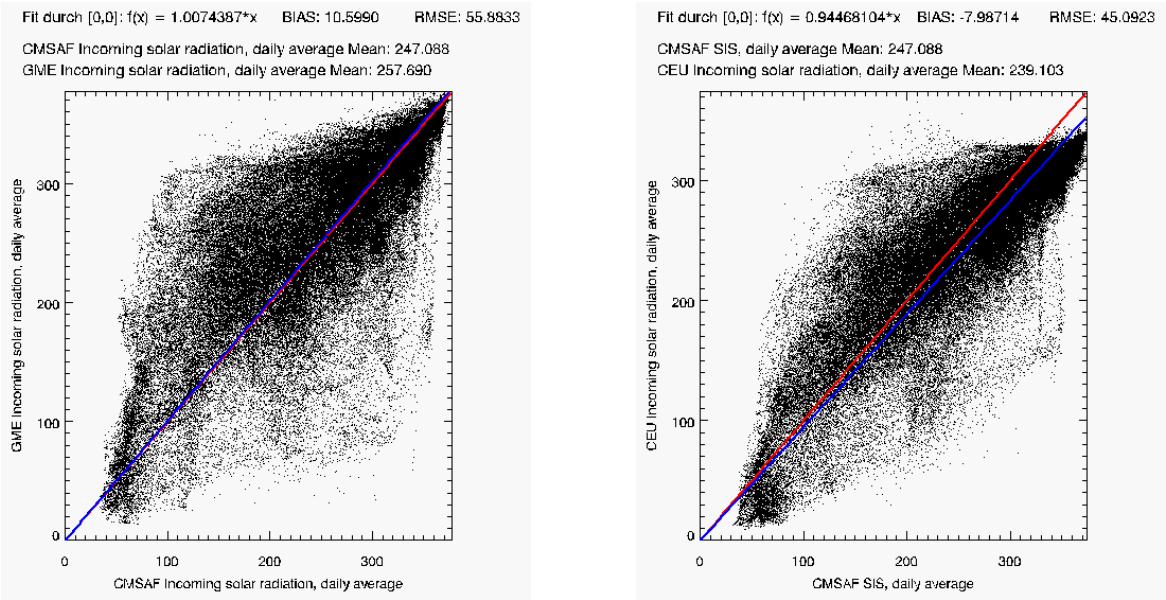

Figure 13: Comparison of the daily averaged solar incoming radiation at surface from the satellite retrieval of CMSAF with GME (left) and COSMO-EU (right) for the 1st June 2013.

4.5 Conclusions

The long-term objective verification over 3 months indicates that considering the global skill the experimental setup improves the operational COSMO-EU in various parameters. However, the question of the increased 2 m-temperature bias and RMSE of the experiment compared to the operational setup remains.

A recent comparison of the satellite retrieval of daily averaged short-wave incoming radiation at surface with COSMO-EU (Fig. 13, right) showed for the operational setup the expected underestimation of incoming solar radiation for cloud-free conditions, i.e. high values of solar radiation, and confirms the conclusions from results of the case study for the 10th April 2011 (Fig. 2, bottom). The comparison with GME supports the application of the aerosol climatology since GME's incoming surface fits better to the satellite retrieval in cloud-free conditions. However an overestimation of solar radiation by COSMO-EU occurs in the intermediate range of incoming solar radiation, corresponding to cloudy conditions. The application of the aerosol climatology with decreased aerosol optical depth in that radiation regime is counterproductive, since it enforces the solar radiation at surface and results in increased 2 m-temperature bias in the experimental setup. Therefore, further investigations are needed to improve the model solar radiation at surface in cloudy conditions.

4.6 Summary and Outlook

This study investigated current uncertainties in the description and simulation of surface characteristics that exist for global and limited area models. The critical issue of the limited knowledge of the external parameters and differences in the soil-vegetation atmosphere transfer model TERRA was considered in numerical experiments with GME and COSMO-EU. These experiments at global and regional scale employed a unified configuration of TERRA. A case study of 36 hours forecasts at 10th April 2011, 12 UTC was used to show the interrelationship between external parameters (e.g. vegetation, aerosol optical depth), surface

radiation budget, fluxes of sensible and latent heat, soil moisture, and screen level (dew point) temperature. For clear-sky conditions it was shown that COSMO-EU with the new configuration improves the agreement with SYNOP measurements compared to the operational setup. Based on 24 hours forecasts of soil-moisture analysis monitoring in Europe a long-term comparison of the behavior of TERRA in spring and summer with the new configuration was performed for the global model GME. It was shown that in connection with a decreased warm 2 m-temperature bias in summer, the SMA diminishes their activity for the experiment by reducing the soil water increments in top and bottom SMA layers, while the soil moisture shows the expected decrease in summer. This improvement on the global scale was traced back to a more realistic behavior of TERRA in the experimental configuration and it is expected that this remains valid in the COSMO-EU. The long-term verification of the COSMO experiment showed an improved global skill compared to the operational setup but further progress is expected after improvement of the surface solar radiation forcing in COSMO for cloudy conditions.

References

Tegen, I., Hollrig, P., Chin, M., Fung, I., Jacob, D., and J. Penner, 1997. Contribution of different aerosol species to the global aerosol extinction optical thickness: Estimates from model results. *J. Geophys. Res.*, **102**, 23895–23915.

Tanre, D., J. F. Geleyn, and J. Slingo, 1984. First results of the introduction of an advanced aerosol-radiation interaction in the ECMWF low resolution global model, in Aerosols and Their Climatic Effects. *Proceedings of the Meetings of Experts, Williamsburg, Va., 28-30 March 1983, edited by H. E. Gerber and A. Deepak, A. Deepak, Hampton, Va*, 133–177.

Hohenegger, C., and P. L. Vidale, 2005. Sensitivity of the European climate to aerosol forcing as simulated with a regional climate model. *J. Geophys. Res.*, **110**, D06201.

Moody, E. G., King, M. D., Schaaf, C. B., and S. Platnick, 2008. MODIS-Derived Spatially Complete Surface Albedo Products: Spatial and Temporal Pixel Distribution and Zonal Averages. *Journal of Applied Meteorology and Climatology*, **47(11)**, 2879–2894.

Balsamo, G., Viterbo, P., Beljaars, A., van den Hurk, B., Hirschi, M., Betts, A. K., and K. Scipal, 2009. A Revised Hydrology for the ECMWF Model: Verification from Field Site to Terrestrial Water Storage and Impact in the Integrated Forecast System. *J. Hydrometeor.*, **10**, 623–643.

Lange, M., 2011. Einführung der Bodenfeuchteanalyse (SMA) für GME. Änderungsmitteilung operationelles NWV-System, Deutscher Wetterdienst, Offenbach.

Ritter, B., 2007. Einführung GME-Version 2.13. Änderungsmitteilung operationelles NWV-System Deutscher Wetterdienst, Offenbach.

Scipal, K., Drusch, M., Wagner, W., 2008. Assimilation of a ERS scatterometer derived soil moisture index in the ECMWF numerical weather prediction system. *Advances in Water Resources*, **31**, 1101–1112.

Masson, V., Champeaux, J.-L., Chauvin, F., Meriguet, Ch., and R. Lacaze, 2003. A Global Database of Land Surface Parameters at 1-km Resolution in Meteorological and Climate Models. *J. Climate*, **16**, 1261–1282.

Doms, G., Förstner, J., Heise, E., Herzog, H.-J., Raschendorfer, M., Schrodin, R., Reinhardt, Th., and G. Vogel, 2005. A description of the Nonhydrostatic Regional Model LM, Part II: Physical parameterization. See: www.cosmo-model.org

4.7 Appendix

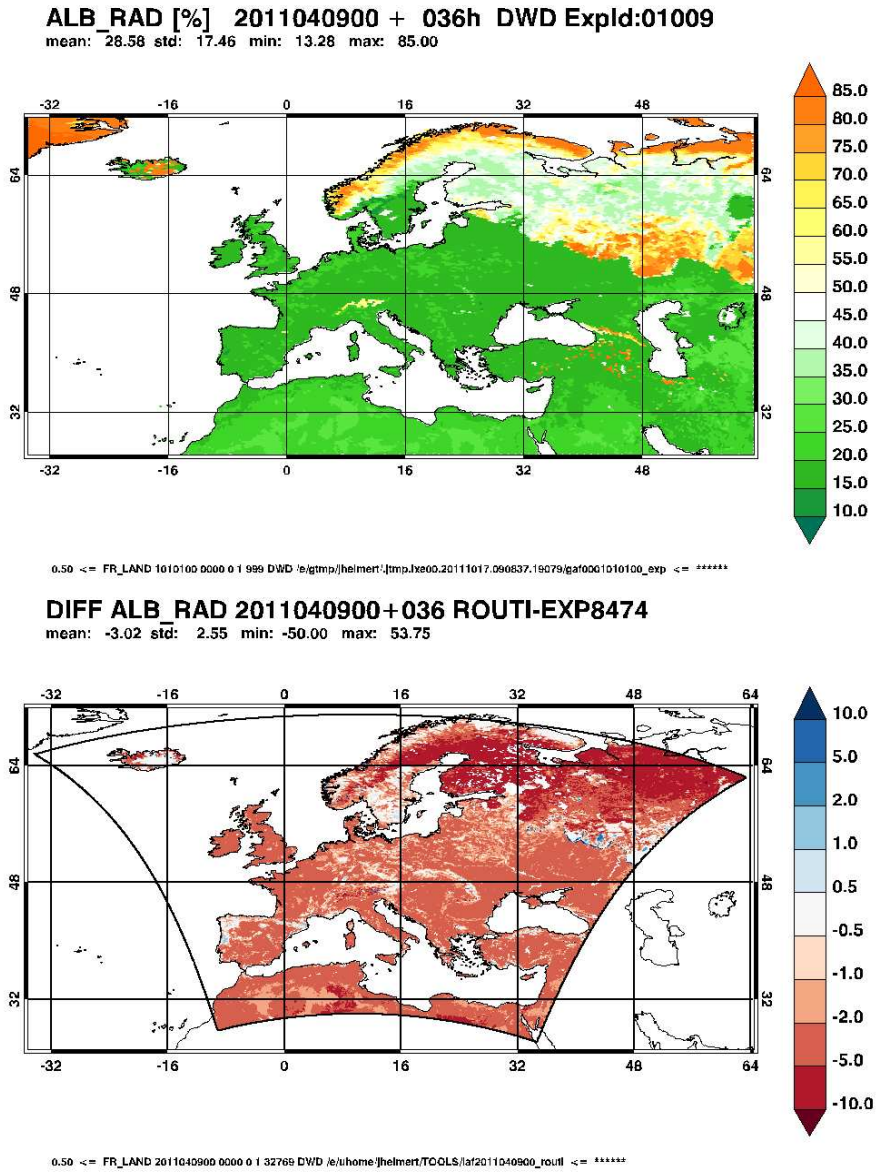

Figure 14: Surface albedo (%) at 10th April 2011 12 UTC for 36 hours forecast of the GME experiment 109/1009 (top) and difference between COSMO-EU routine and experiment 8474 (bottom).

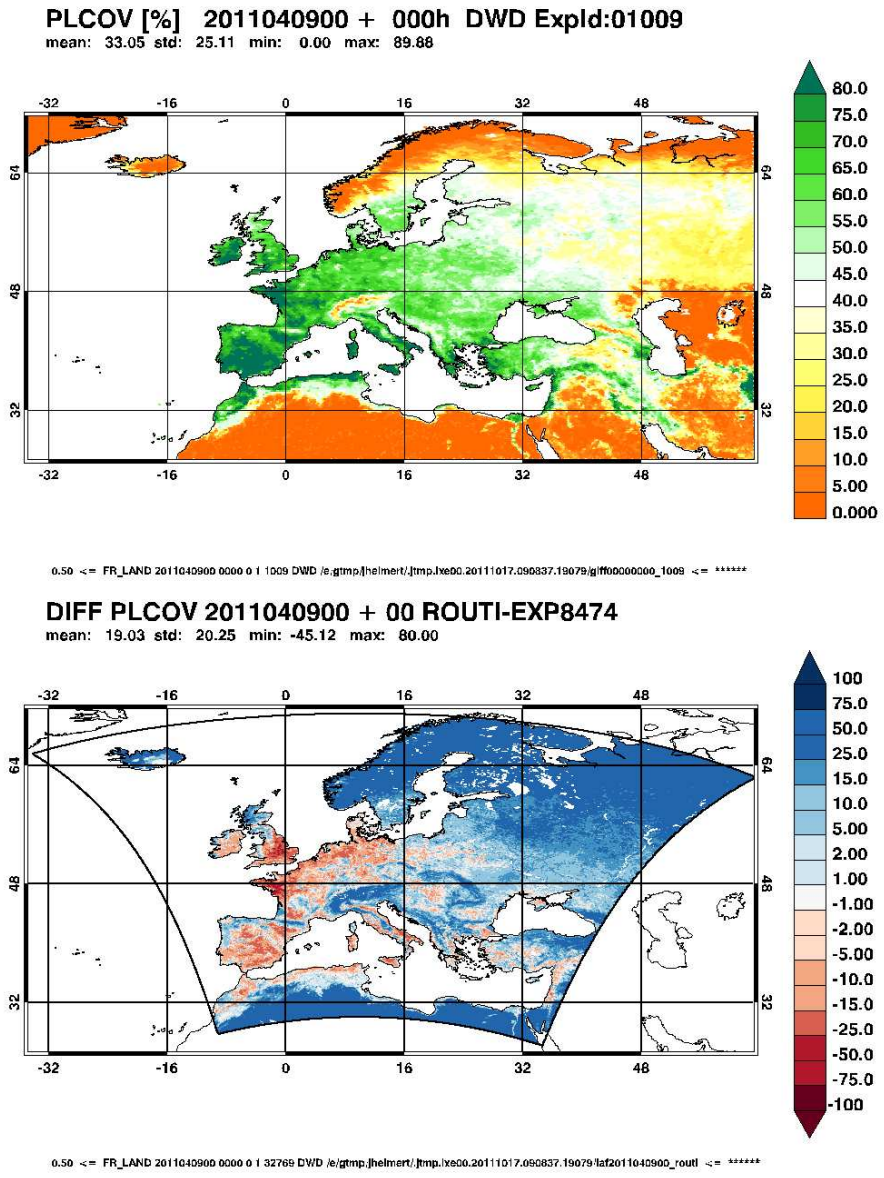

Figure 15: Vegetation coverage (%) at 9th April 2011 00 UTC of the GME experiment 109/1009 (top) and difference between COSMO-EU routine and experiment 8474 (bottom).

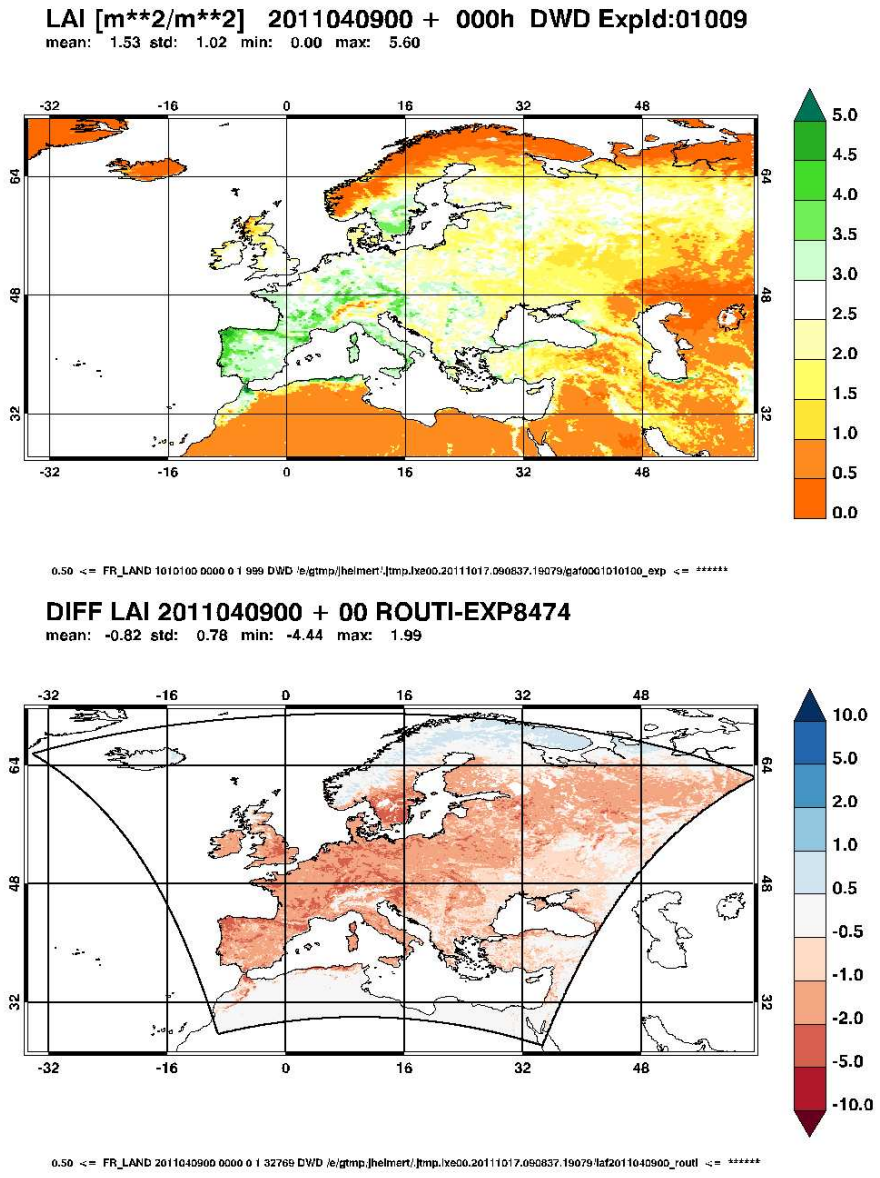

Figure 16: Leaf area index at 9th April 2011 00 UTC of the GME experiment 109/1009 (top) and difference between COSMO-EU routine and experiment 8474 (bottom).

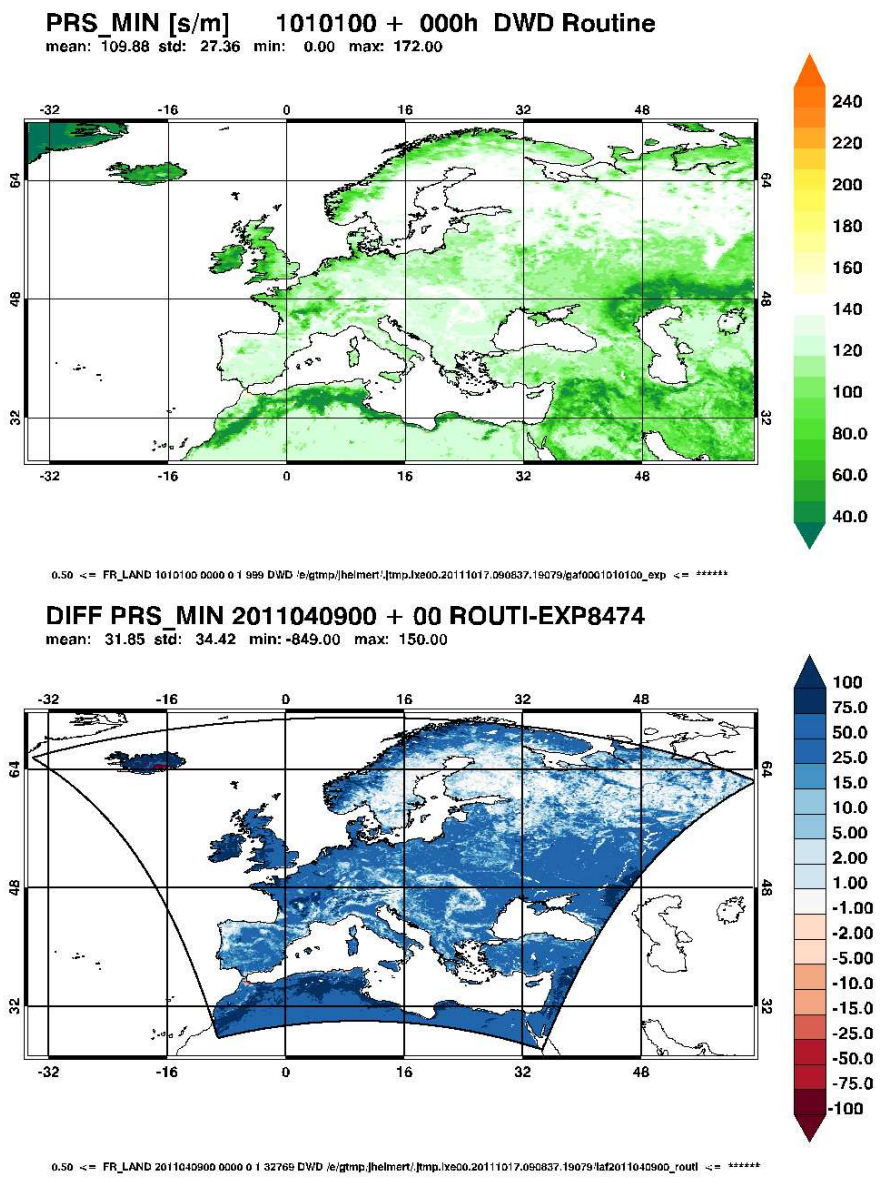

Figure 17: Minimum stomatal resistance ($sm^{-}1$) of the GME experiment 109/1009 (top) and difference at 9th April 2011 00 UTC between COSMO-EU routine and experiment 8474 (bottom).

5 Documentation of a new multi-layers snow module (E. Machulskaya)

The snow model that is presented here is a one-dimensional parameterization scheme for the heat and moisture transfer through the snowpack. Two main features of the scheme distinguish it from the snow parameterization scheme that is currently operational in COSMO. First, it allows the water to be in the liquid state within snowpack. Second, the new scheme is multi-layered, i.e. the vertical profiles of temperature, total and liquid water content, and density are explicitly resolved.

The heat and moisture transport through the snowpack is governed by the following set of equations

$$\begin{aligned}
\rho_{sn} C_{sn} \frac{\partial T_{sn}}{\partial t} &= \frac{\partial}{\partial z} \lambda_{sn} \frac{\partial T_{sn}}{\partial z} + L_f (F - M) - \frac{\partial R}{\partial z} \\
\frac{\partial W_{liq}}{\partial t} &= M - F - \frac{\partial q}{\partial z} \\
\frac{\partial W_{tot}}{\partial t} &= -\frac{\partial q}{\partial z} \\
\frac{\partial \rho_{sn}}{\partial t} &= \frac{\rho_{sn}}{W_{tot}} \left(-\frac{\partial q}{\partial z} \left(1 - \frac{\rho_{sn}}{\rho_w} \right) + \rho_{sn} \frac{\rho_w - \rho_i}{\rho_w \rho_i} (M - F) \right) + \sigma(t),
\end{aligned} \tag{1}$$

where T_{sn} is snow temperature, W_{liq} is specific liquid water content, W_{tot} is specific total water (liquid + solid) content, C_{sn} is specific heat capacity of snow, ρ_{sn}, ρ_w and ρ_i are densities of snow, water and ice, respectively, λ_{sn} is snow heat conductivity, L_f is latent heat of freezing, M and F are melting and refreezing rates, respectively, q is the liquid water flux, R is radiative heat flux, and $\sigma(t)$ characterizes the impact of gravitational compaction and metamorphism on snow density.

The first equation is an expression for the energy conservation law. As can be seen, snow temperature changes may be caused by the heat diffusion, latent heat release due to water phase changes (melting of solid part and refreezing of liquid part), and solar radiative heating that can occur not only at the upper snow surface, but also below it. The second equation is the expession for the liquid water balance; the liquid water content may change because of phase changes and percolation of water. The third equation is the total snow water-equivalent balance equation. The fourth equation describes the changes in the snow density. The first and the second terms on the right-hand side of this equation describe the change in snow density due to the changes of the ratio of the solid part (of the ice density) to the liquid part (of the water density). It may occur either because some amount of water is percolated from above (the first term) or because of phase changes (second term). The third term describes the densification of the snowpack due to the weight of the overlying layers and due to internal metamorphism.

Snow heat capacity C_{sn} is computed as

$$C_{sn} = W_{liq} \rho_w C_w + (W_{tot} - W_{liq}) \rho_{dry} C_i,$$

accounting for liquid water content. Here, ρ_{dry} is the density of the solid part of a snow layer and it is equal to

$$\rho_{dry} = \frac{W_{tot} - W_{liq}}{\frac{\rho_w}{\rho_{sn}} W_{tot} - W_{liq}} \rho_w.$$

Snow heat conductivity λ_{sn} depends on snow density and varies therefore with height and time. It is calculated by means of an empirical formula

$$\lambda_{sn} = 2.22 \left(\frac{\rho_{sn}}{\rho_i} \right)^{1.88}.$$

The liquid water flux q consists of precipitation flux at the upper boundary of snow which is provided by the host atmospheric model as an upper boundary condition, and of the flux due to the internal percolation of liquid water within the snowpack. Percolation flux is calculated according to (Colbeck, 1978) as

$$q = \rho_w h \max \left(\left(\frac{W_{liq}/\rho_w - W_{hc}}{\Pi - W_{hc}} \right)^3, 0.0 \right),$$

where $W_{hc} = 0.04$ m^3/m^3 is the volumetric water holding capacity of snow, $h = 0.01$ m/s is snow hydraulic conductivity by maximal liquid water content W_{hc}, and

$$\Pi = 1 - \frac{W_{liq}}{\rho_w} - \frac{W_{tot} - W_{liq}}{\rho_i}$$

is the snow porosity. The percolation flux through the lower boundary of the snowpack is regarded as net snow melting rate and it is used as the upper boundary condition for soil moisture by the soil model.

Radiative heat flux is calculated according to exponential extinction law

$$R(z) = R_0 e^{-\beta z},$$

where R_0 is the net solar radiation flux at the snow-air interface and β is the extinction coefficient. The latter is assumed to be dependent on snow density. A simple linear dependence was constructed based on the data reported in literature

$$\beta = b_1 \rho_{sn} + b_2,$$

where $b_1 = 0.13$ and $b_2 = 3.4$, so that $\beta = 10$ m^{-1} if snow density is 50 kg/m^3 and $\beta = 70$ m^{-1} if snow density is 500 kg/m^3 (fresh snow is more penetrable to sunlight).

Gravitational compaction and compaction due to metamorphism are described by means of the following semi-empirical law:

$$\sigma(z,t) = \frac{\rho_{sn}(z,t)}{\eta(z,t)} \left(\sigma_g(z,t) + \sigma_m(z,t) \right).$$

Here, σ_g describes the effect of gravity and it is equal to the total weight of the overlying layers

$$\sigma_g(z,t) = \int_0^z \rho_{sn}(z') g dz'.$$

The term σ_m describes the compaction due to metamorphism. It is set to a constant value $\sigma_m(z,t) = 75$ Pa.

The factor $\eta(z,t)$ is the compactive viscosity of snow that characterizes the proneness of the snowpack to the deformations due to both abovementioned processes. It is equal to

$$\eta(z,t) = A_1 \exp \left(A_2 \frac{\rho_{sn}(z,t)}{\rho_i} - a W_{liq}(z,t) + \frac{E}{R T_{sn}(z,t)} \right),$$

where $A_1 = 6.6 \cdot 10^{-7}$ Pa $\cdot$ s, $A_2 = 19.3$, $a = 70.0$, $E = 67300$ J/mol is the activation energy and $R = 8.31$ J/(mol K) is the universal gas constant. As can be seen, three characteristics of the snowpack determine its ability to densify: the snow density, liquid water content and snow temperature. The incompacter, warmer, and moister the snowpack is, the easier it shrinks.

Boundary conditions. Since the equation for temperature is of the second order and all other equations of the first order, the first equation requires two boundary conditions, and all other one boundary condition. The upper boundary condition for the temperature transport equation is the heat flux at the snow-air interface, as in the single-layer snow model. The total heat flux is the sum of net solar and infrared radiation, sensible and latent heat fluxes, heat conduction flux into snowpack and the flux of heat which is released by the freezing rain that falls onto the snow surface. Note that the latter flux is not present in the total heat balance in the single-layer snow model.

The upper boundary condition for the total water content also appears in the flux form. It is the precipitation flux, either in the form of snow or in the form of rain. The latter serves also as the upper boundary condition for the equation for liquid water content.

The lower boundary condition for temperature is the conductive heat flux through the soil-snow interface.

The density of the upper surface of the snowpack is determined by the falling snow density. This fresh snow density is calculated as in the single-layer snow model, namely

$$\rho_{fr} = \rho_{frmin} + (\rho_{frmax} - \rho_{frmin}) \frac{T_{air} - T_{min}}{T_0 - T_{min}},$$

where $\rho_{frmin} = 50$ kg/m^3, $\rho_{frmax} = 150$ kg/m^3, $T_{min} = 258.15$ K = 273.15 - 15.0 K, $T_0 =$ 273.15K. It is an increasing function of temperature that emulates heavy "moist snow" if the air temperature is close to the melting point.

Numerical implementation. **Time discretization.** The equation system (1) is solved by means of splitting up method. At the first half time step the heat diffusion is calculated (implicitly), at the second half time step the adjustment is made due to the presence of sources and sinks (explicitly).

The adjustment of the snow temperature and total and liquid water content profiles due to phase changes is made in the one-iteration way. Specifically, if after the temperature diffusion half-step snow temperature T^*_{sn} becomes greater than the melting point $T_0 = 273.15$K, melting is detected ($M > 0$). In this case, if the heat storage excess that should be spent on melting $E = C_i W_{tot}(T^*_{sn} - T_0)\rho_w$ is enough to melt the entire solid part of the layer $W_{tot} - W_{liq}$ (i.e. $E \geq L_f \rho_w (W_{tot} - W_{liq})$), then the melting rate is $M = (W_{tot} - W_{liq})/dt$, the whole layer becomes liquid ($W_{liq} = W_{tot}$), and the rest of energy is transferred into the underlying layer. Otherwise, if the heat stored in the layer is not enough to melt the entire solid part of the layer, it is spent to melt a part of it, the melting rate is then $M = C_i W_{tot}(T^*_{sn} - T_0)/(L_f dt)$ and liquid water content increases by $W_{liq} = W_{liq} + C_i W_{tot}(T^*_{sn} - T_0)/L_f$. In both cases, the temperature of the layer is set to $T^{new}_{sn} = T_0$.

Refreezing rate F is calculated in a similar way. $F > 0$ if the temperature of a layer T^*_{sn} after the diffusion half-step becomes less than the melting point T_0 but some amount of liquid water is present. In this case, if T^*_{sn} is low enough that the whole amount of liquid water can refreeze (i.e. $E = C_i W_{tot}(T_0 - T^*_{sn})\rho_w \geq L\rho_w W_{liq}$), then the new liquid water content is $W^{new}_{liq} = 0$ and temperature of the layer increases by latent heat release as $T^{new}_{sn} = T^*_{sn} + W_{liq} L_f/(W_{tot} C_i)$. Otherwise, if not all the liquid water can freeze, then a part

of it freezes, namely, W_{liq} becomes $W_{liq}^{new} = W_{liq} - C_i W_{tot}(T_0 - T_{sn}^*)/L_f$ and temperature T_{sn}^{new} is set to T_0.

Space discretization. The vertical grid consists of a constant number of layers that is fixed by user with setting the name-list variable *ke_snow*. At each time step the thickness of a layer can change:

1) due to changes in snow density of the layer whereas the total mass of the layer conserves but phase changes occur;

2) due to mass flux as some amount of water percolates from the overlying layer and/or into the underlying layer;

3) the thickness of the uppermost layer can increase if fresh snow has fallen.

Due to these processes the vertical grid becomes irregular even if it is regular at the initial time step. Thus, at the end of the time step a regularization is performed in order to return the grid to the regular one. This procedure sets new equidistant heights of layers and linearly interpolates snow temperature, density, total water and liquid water content values from the old grid to the new one.

To switch between the single-layer and multi-layer snow model the name-list logical variable *lmulti_snow* is used.

6 Implementation of the Martilli Urban Surface Parametrization in COSMO (O. Fuhrer, C. Muller, G. Fontannaz)

6.1 Introduction

Meteorological information has become more and more important in our society, as many activities and life being are largely influenced by the weather. For example, air and maritime transport security, air quality control, global change study, natural disaster forecast, water resources management or simply freetime activities require meteorological forecast and/or analysis. Our capacity to forecast the weather has hence became a great issue. Today half of the worlds' population lives in urban areas, where a wide variety of human activities takes place. Meteorological forecast needs are very important for urban area even if it represents only 0.05 % of the Earth's surface. In order to answer at best to these needs, the numerical forecast models are used. The quality of the information delivered by such models are strongly dependent on their resolution. During the last decade, computers performances have strongly increased, making it possible to constantly improve the model resolution. Being able to take into account finer scale and hence smaller geomorphological features, we could expect an improvement of the model results accuracy. However, results are only improved when different parametrizations, which take into account subgrid effects and the Earth's surface representation (landuse), are regularly updated to fit with the increasing resolution.

Concerning the Earth's surface fluxes exchanged with the atmosphere, increase of the model resolution have led to the adaptation of surface exchange parametrizations to take into account urbanized areas reproduced in mesoscale models by high resolution landuse database. Different solutions are available in order to parametrize the urban area in weather forecast models. The most common is based on the Monin-Obukhov Similarity Theory (MOST), which assumes that a stable surface layer develops above the ground and where turbulence is constant in time and space. A more sophisticated solution is to use Urban Canopy Models (UCM), where the surface fluxes are solved by taking into account buildings, different surfaces of city (roof, road and wall) and their interactions with the atmosphere (Martilli et al., 2002; Masson, 2000). In this study, we investigate the capacity of two parametrization (a MOST based scheme and an UCM) to reproduce the urban area effects in a Numerical Weather Prediction (NWP) model. We focus on the Urban Heat Island (UHI) which is a typically phenomenon for urban areas and relatively easy to measure and quantify. For this purpose, the model of the Swiss Federal Office of Meteorology and Climatology (MeteoSwiss) is used. This mesoscale model called Local Model (LM) uses a traditional urban area parametrization (dry soil and adapted surface roughness) based on MOST. It is used for operational numerical weather prediction since 2001 with a horizontal resolution of 7 km on a domain covering most of western Europe.

In order to see if LM is able to reproduce the urban effect, it is applied to the City of Basel, a mid-size city situated in Switzerland, where an extensive meteorological measurement campaign has been conducted in the city of Basel under the BUBBLE project (Basel UrBan Boundary Layer Experiment) (Rotach et al., 2005) from summer 2001 to summer 2002. This experiment investigates in detail the boundary layer structure over a city. Different modeling studies have been conducted in relation with this experiment (Roulet, 2004; Hamdi, 2005), but none of them with an operational model able to take into account numerous phenomenon, *i.e.* clouds, rain, snow, etc. In this report, the ability of LM to reproduce urban effects, and more particularly the UHI, is evaluated using BUBBLE measurement data as reference, first with the operational configuration of the model, and then with a finer horizontal and vertical resolution. In a second step, we focus on an urban canopy model developed by Martilli et

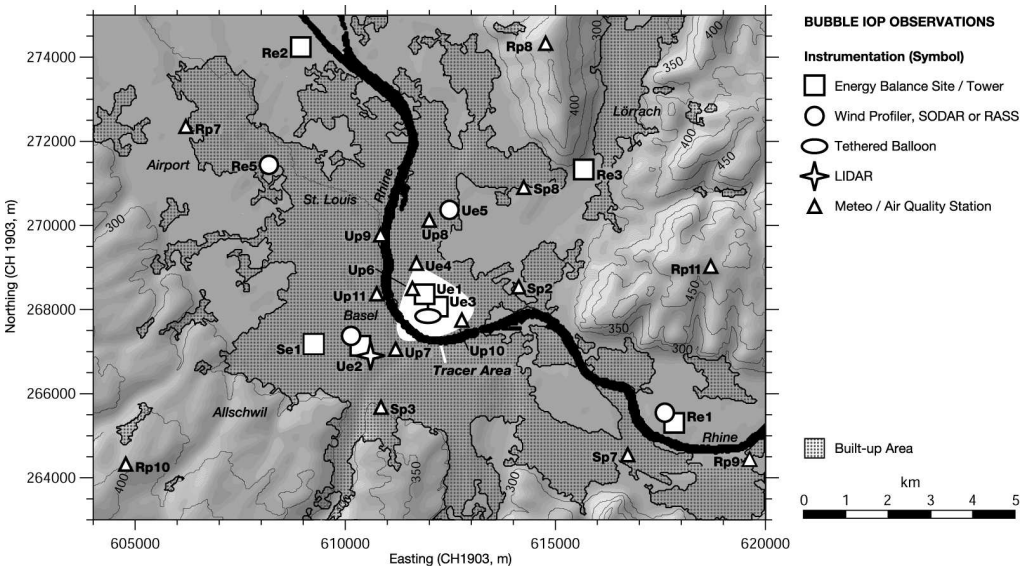

Figure 18: Map of the greater area of the city of Basel with an overview of all sites operated during the BUBBLE IOP in June/July 2002. The thick black line denotes the river Rhine. A complete list of the measuring stations can be found in Appendix 6.9.1

al. (2002). This Urban Effects Parametrization (BEP) is presented and implemented into LM. This implementation and its ability to reproduce the urban effects in LM for the case of Basel city are then evaluated and discussed.

6.2 Bubble

6.2.1 The Experiment

The City of Basel is located in the North-Western part of Switzerland and borders both France and Germany. It is the Switzerland's third most populous city with 190,000 inhabitants. It is situated on the Rhine river, at an altitude of about 260 m and surrounded by gentle but non-negligible topography (750m).

The Basel UrBan Boundary Layer Experiment (BUBBLE) took place from August 2001 to July 2002. Its main goal is to study boundary-layer and surface-exchange processes over different types of surfaces (*i.e.* urban, sub-urban and rural) and their role in the transport and diffusion of air pollution. A more complete description of BUBBLE can be found in Rotach et al. (2005) and on the BUBBLE website. For that purpose, two meteorological towers for turbulence measurements, a Lidar and wind profiler were operated. An Intensive Observation Period (IOP) took place from 15 June and 12 July 2002, with additional surface towers, sodars and tethered balloons (Fig. 18).

6.2.2 Measurements of the UHI

In contrast to rural area, a city represents a dry surface with obstacle (buildings) and a source of anthropogenic heat. The urban area modifies the energy budget, thus creating meteorological differences between urban and rural area. These dissimilarities can be formulated as the differences between urban and rural air temperatures, the first one being usually higher. This phenomenon is called the Urban Heat Island (UHI). As a UHI indicator, averaged and height corrected surface temperature observations within the city are

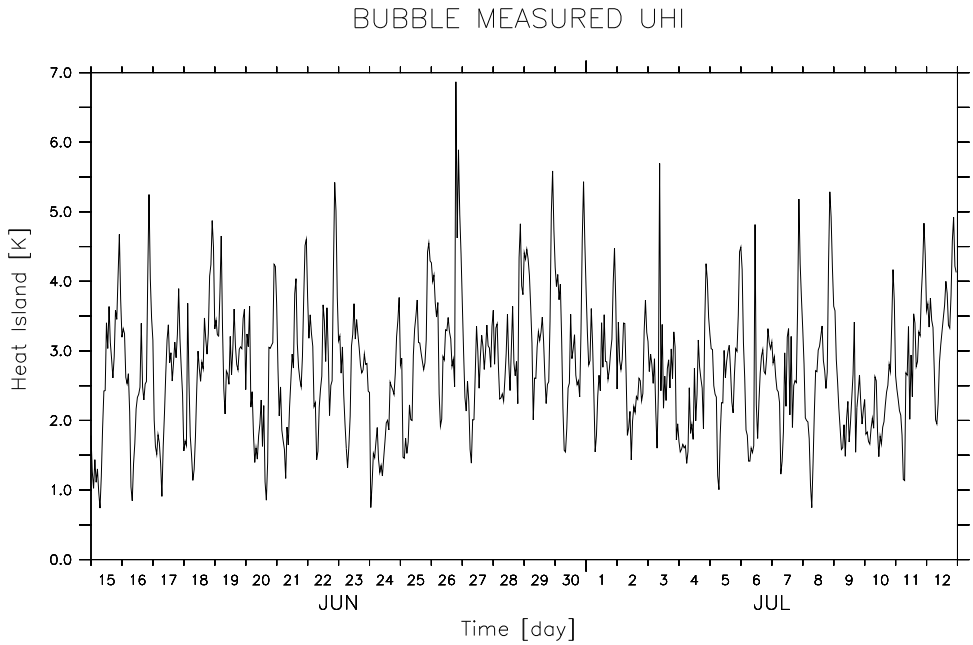

Figure 19: The UHI measured for the city of Basel at 2mAGL during the BUBBLE IOP in June/July 2002

compared with measurements from surroundings rural areas. The BUBBLE campaign provide temperature measurements at 2 m height on several representative sites for urban or rural conditions. Averaging temperature in both areas (urban and rural) allow to obtain a temperature difference between the city and its surroundings, which can be assimilated to the UHI. Figure 19 shows this averaged temperature difference between urban and rural area measured during the IOP. It is always positive and varies from 0.7 to 6.9 °C with an average of 2.8 °C. If we look at the weather bulletin (Appendix 6.9.2) during the IOP, the period from 25 to 27 June is characterized by a very constant meteorological situation and strong daily cycle. The mean UHI over this episode is representative for the IOP with an average of 3.0 °C. This episode is used to study UHI formation over Basel. Furthermore, it corresponds to the period studied by Roulet (2004).

In the following, an in-depth analysis of this UHI episode using measurements and numerical simulations is presented.

6.3 The COSMO Model

6.3.1 Model Description

The LM (Lokal-Modell[1]) is developed within the framework of the COnsortium for Small-Scale MOdeling (COSMO) bringing together the National Weather Services from Switzerland, Italy, Poland and Greece under the lead of the National Weather Service of Germany (DWD). LM is a nonhydrostatic fully compressible limited-area atmospheric model. It has been designed for both operational Numerical Weather Prediction (NWP) and various scientific applications on the meso-β and meso-γ scales (scales from which the nonhydrostatic effects begin to play an important role on the behavior of the atmospheric fluxes (Orlanski, 1975). The LM prognostic variables are horizontal and vertical cartesian wind compo-

[1]A more detailed description of the LM can be found on the COSMO website.

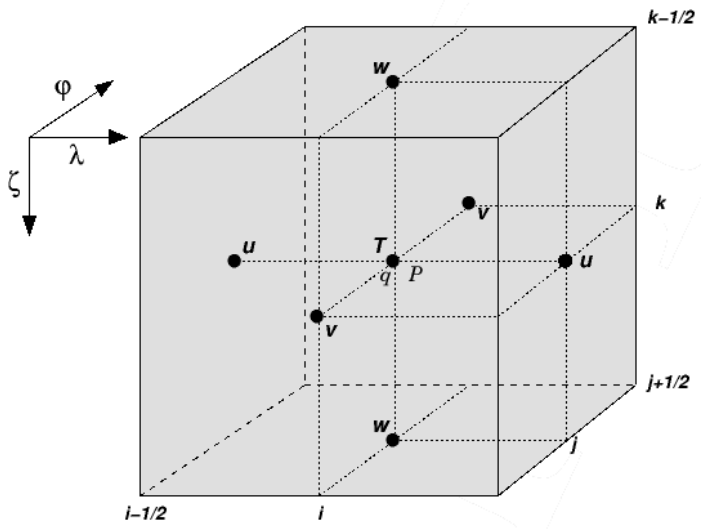

Figure 20: A grid box volume $\Delta V = \Delta\lambda\Delta\phi\Delta\zeta$ showing the *Arakawa-C/Lorenz* staggering of the dependent model variables. The scalar variables T, P and q are defined at the centre (i, j, k) of the box, whereas the normal velocity components are defined on the corresponding box faces $(i \pm 1/2, j \pm 1/2, k \pm 1/2)$.

nents, temperature, pressure perturbations, specific humidity, as well as different cloud water species and turbulence quantities according to the parametrizations chosen for the phenomena. The model is based on the primitive thermo-hydrodynamical equations describing a compressible flow in a moist atmosphere. The model equations are formulated horizontally in rotated geographical coordinates (λ, ϕ) and vertically in a generalized terrain following height coordinate (ζ). These equations are solved numerically using finite difference methods in an Arakawa-C/Lorenz grid (Figure 20 shows a grid box volume). Constant increments $\Delta\lambda, \Delta\phi, \Delta\zeta$ are used to set up the computational grid and the domain is represented by a finite number of grid points (i, j, k). Each of these points is the center of a rectangular grid box volume $\Delta V = \Delta\lambda\Delta\phi\Delta\zeta$.

NUMERICAL INTEGRATION

(a) The Time Integration Scheme

To illustrate the integration used in LM, let consider the model equations in the generic form

$$\frac{\partial\psi}{\partial t} = s_\psi + f_\psi, \tag{2}$$

where ψ denotes a prognostic model variable (u, v, w, T, p' or q), f_ψ the forcing terms due to the slow modes and s_ψ the source terms related to the acoustic and gravity wave modes. Equation 2 is solved using a Kemp-Wilhelmson time-splitting algorithm, where terms related to the slow modes are solved using a large time step dt, whereas the acoustic and gravity waves modes are solved using a small time step $d\tau$. The slow-mode forcing f_ψ is evaluated only once every large time step and kept constant throughout the small time steps, whereas the fast-mode terms contained in s_ψ are calculated for each small time step.

We focus on the turbulent fluxes of heat and momentum which are contained in the slow mode term f_ψ. Horizontal advection is treated explicitly and evaluated at mid-time level n, whereas diffusion evaluated at time level n would be unstable with respect to explicit *Leapfrog* integration scheme. Thus, the computational mixing terms are formulated following a simple forward scheme, *i.e.* they are evaluated at the time level $n-1$. Vertical advection and vertical

turbulent diffusion are treated implicitly using the *Crank-Nicolson* scheme involving the time levels $n-1$ and $n+1$. This results in a vertically coupled set of equations, abbreviated by

$$\frac{\psi^{n+1}-\psi^{n-1}}{2\Delta t} = f_\psi^n = f_\psi(\psi^{n-1}, \psi^n, \psi^{n+1}) \tag{3}$$

Finally for the slow mode tendency $\tilde{\psi}^{n+1}$, evaluating the finite difference equations for u, v, w, T, $p^{'}$ and q from (3) enables to obtain a linear tridiagonal equations system, which may be written in the general form

$$A_k\tilde{\psi}_{k-1}^{n+1} + B_k\tilde{\psi}_k^{n+1} + C_k\tilde{\psi}_{k+1}^{n+1} = D_k(\psi^n, ...), \tag{4}$$

for variables defined on main levels by k ($k = 1, ..., N_\zeta$). Boundary conditions are included in the inhomogeneous term D_k. Thus, we end up with a tridiagonal matrix of dimension $(N_\zeta) \times (N_\zeta)$, which can be solved by Gaussian elimination in LM.[2]

(b) Land-Surface Scheme

The turbulent mixing terms for temperature, moisture variables and horizontal momentum (in both directions u and v) are related respectively to the turbulent fluxes of sensible heat ($\hat{H}^3$), moisture (F_q^3) and momentum (τ^{13} and τ^{23}) respectively. These fluxes are defined at model half levels and at the horizontal position corresponding to the transported quantity. The calculation of the mixing terms requires boundary conditions for turbulent fluxes at the top ($\zeta = 1/2$) and at the bottom ($\zeta = N_\zeta + 1/2$) half level of the model , where N_ζ is the number of vertical levels. At the upper boundary, zero flux conditions are specified:

$$\begin{aligned}(\tau^{13})_{\zeta=1/2} = (\tau^{23})_{\zeta=1/2} &= 0,\\ (\hat{H}^3)_{\zeta=1/2} = (F_q^3)_{\zeta=1/2} &= 0\end{aligned} \tag{5}$$

At the lower boundary, the turbulent fluxes are specified which a standard bulk-transfer scheme using a drag-law formulation [3]:

$$\begin{aligned}(\tau^{13})_{\zeta=N_\zeta+1/2} &= \tau_{sfc}^{13} = -\rho C_m^d|\vec{v}_h|u,\\ (\tau^{23})_{\zeta=N_\zeta+1/2} &= \tau_{sfc}^{23} = -\rho C_m^d|\vec{v}_h|v,\\ (\hat{H}^3)_{\zeta=N_\zeta+1/2} &= \hat{H}_{sfc}^3 = -\rho C_h^d|\vec{v}_h|(\theta\pi_{sfc} - T_{sfc}),\\ (F_{q^v}^3)_{\zeta=N_\zeta+1/2} &= (F_{q^v}^3)_{sfc} = -\rho C_h^d|\vec{v}_h|(q^v - q_{sfc}^v),\end{aligned} \tag{6}$$

where u, v, θ and q^v are the horizontal velocity components, the potential temperature and the specific humidity at the lowest grid level above the surface ($\zeta = N_\zeta$). $|\vec{v}_h|$ is the absolute horizontal wind speed at the same level. C_m^d denotes the drag coefficient for momentum exchanges at the ground and C_h^d is the bulk-aerodynamical transfer coefficient for turbulent heat. The transfer coefficient for moisture is assumed to be equal to the one for heat in LM. The air density ρ is evaluated from the surface values for temperature, pressure and humidity. Temperature and specific humidity at the ground are either provided by the soil model or externally specified, whereas the surface pressure is determined by hydrostatic extrapolation of the total pressure $p = p_0 + p^{'}$ at the first layer above the ground. The transfer coefficients C_m^d and C_h^d are calculated diagnostically and derived from the Monin-Obukhov Similarity Theory (MOST). Similarity theories are empirical relationships for variables of interest when our knowledge of the governing physics is insufficient to derive laws based on first principles (Stull, 1988). MOST is a first order approximation usually applied to the surface layer and assumes constant fluxes. Thus, in order to apply MOST for surface fluxes parametrization,

[2]The matrix diagonal terms A_k, B_k and C_k, as well as the D_k-term are derived in Doms et al. (2002a).

[3]As described in the Part II of the LM documentation (Doms et al., 2002b).

Table 2: Characteristic parameters for urban and built up areas in TERRA_LM: z_0 is the surface roughness.

Land use class	z_0 [m]	root depth [m]	plant cover		leaf area index	
			Max	Min	Max [-]	Min [-]
urban and built up land	1.00	0.60	10%	5%	4.70	0.10

the lowest grid layer of the model must be within the constant-flux layer. Usually, the top of the surface layer in rural areas is in the range of 10m to 30m.

THE SOIL AND VEGETATION MODEL

Surface fluxes represent the lower boundary conditions for the atmospheric part of the model. Their calculation requires temperature and specific humidity as input in the first soil layer predicted by the soil model. For land surfaces, the multi-layer soil model TERRA_LM (Doms et al., 2002b) provides surface temperature and specific humidity at the ground to the LM model. Most parameters of the soil model (heat capacity, water storage capacity, volume of voids, etc.) strongly depend on soil texture. Five different types are distinguished: sand, sandy loam, loam, loamy clay and clay. Three special soil types are considered additionally: ice, rock and peat. The ground temperature is calculated by the equation of heat conduction which is solved in an optimized two-layer model, to which a third layer called the climatological layer, characterized by constant temperature, is added. The urban and built-up land are described as a loam-clay soil with specific parameters described in Table 2. The temperature at 2 m Above Ground Level (AGL) is computed diagnostically from the ground surface temperature and the temperature in the first model layer according to the land-surface scheme *i.e.*, the Monin-Obukhov Similarity Theory.

6.3.2 MeteoSwiss Operational Implementation

Since April 2001, a nonhydrostatic mesoscale model (COSMO), is used at MeteoSwiss for operational Numerical Weather Prediction (NWP). The current (fall 2006) Swiss version of the model has a horizontal resolution of about 7 km. The domain covers most of western Europe. A terrain following vertical coordinate system is used, with 45 vertical layers and about 50 to 100 m vertical resolution in the lowest 2 km of the atmosphere, and an upper level at a geopotential height of 20 hPa. The 2 mAGL temperature is computed according to MOST using the temperature of the first layer and the surface temperature in the model. The operational run of COSMO at MeteoSwiss is performed twice daily, at 1:30 am and 1:30 pm GMT. Calculations are performed on a NEC-SX/5 supercomputer at the Swiss National Supercomputing Center (CSCS) in Manno (TI). A 72 hour forecast takes roughly 70 minutes real-time. Accurate initial conditions are generated with an additional assimilation system, using observations within the model domain (*e.g.* wind profiler). Boundary conditions are taken from the global model of the European Center for Medium-Range Weather Forecasts (ECMWF) in Reading (UK). A new version, called COSMO2, is currently being developed and tested at MeteoSwiss. It will use a horizontal grid-size of roughly 2 km, a more accurate vertical resolution and is planned to become operational at the beginning of 2008.

Table 3: The main model input parameters are: nx and ny the number of urban grid point in each horizontal direction, ny the number of layer on the grid, dx and dy the horizontal grid resolution, dz_{ground} the lowest layer depth and dt the slow modes time step

The main model input parameters	
nx	13
ny	13
nz	45
dx dy	7 km
dz_{groud}	60 m
dt	12 min
episode	25 to 27 June 2002 (72h)

6.3.3 Model Setup

For this study, the operational COSMO configuration is used, with a domain size limited to the Basel area. The computed domain centered on the city of Basel is 13 by 13 grid point for a total surface of 8281 km^2 with a 7 km horizontal resolution. The vertical resolution is 60 m for the lowest model layer. Boundary conditions are taken from the hourly analysis of COSMO computed by MeteoSwiss and are interpolated to our domain. The run lasts 72 hours and covers the 3 days described above, *i.e.* 25 to 27 June, 2002. The main model configuration parameters are summarized in Table 3.

6.4 COSMO vs. Measurements

A general overview of the model performance for the selected episode is presented in this section. In general, the model shows good agreement with the observed meteorological conditions. As the model is driven using analysis for boundary conditions, this is to be expected. In the following, the computed surface fields over the target area, *i.e.* the city of Basel and its immediate rural surroundings, are analyzed and compared to observations. The computed temperature is generally in good agreement with the measurements in rural area. Figure 21 shows the measured temperature averaged over several rural measuring sites (cf. map in Fig. 18) and the computed temperature averaged over the corresponding grid points. The computed maximum temperature at 2 mAGL in rural area occurs one hour earlier and is 0.5°C lower compared to the measurements for the first two days. During nighttime the simulated temperature fits very well to the measurements. However simulated temperature in urban area are too low by 1.5 to 3.0 °C (Fig. 22). The difference between the urban and rural temperature corresponds to the UHI. Figure 23 shows the measured and computed UHI over the city. The averaged computed UHI is 0.14 °C, hence showing no significant temperature difference between urban and rural areas. The temperature in the city is even regularly lower than the temperature in the rural area, particularly during nighttime. As a conclusion, COSMO with the operational configuration is not able to reproduce the UHI and underestimates the magnitude of the urban-rural temperature difference. One possible reason is a too low horizontal and vertical resolution:

- With a 7 km **horizontal resolution**, the city of Basel fills only one grid point; a finer horizontal resolution would allow to represent the city more accurately.
- The COSMO **vertical resolution** used is too low. An accurate representation of

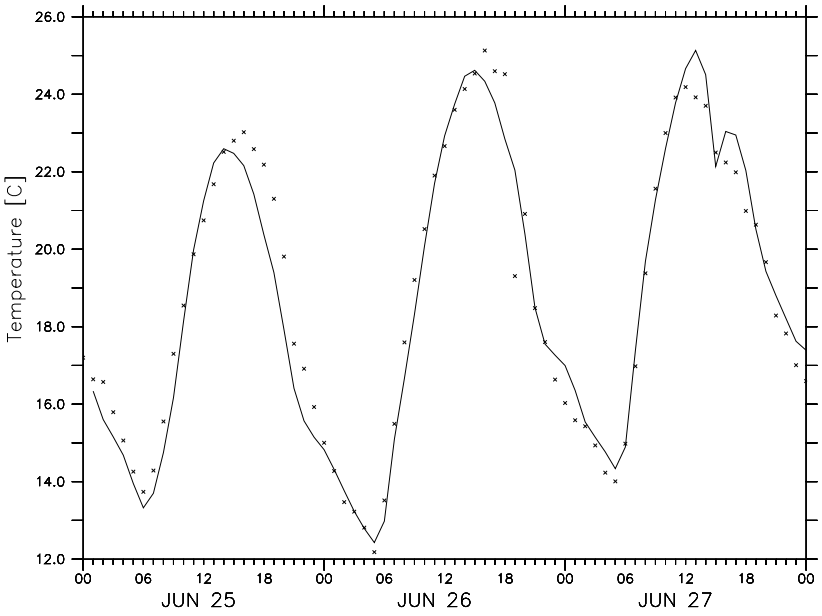

Figure 21: temperature at 2mAGL in rural areas for the period June 25 to 27, measured (crosses) and computed by COSMO (solid line) with the operational configuration.

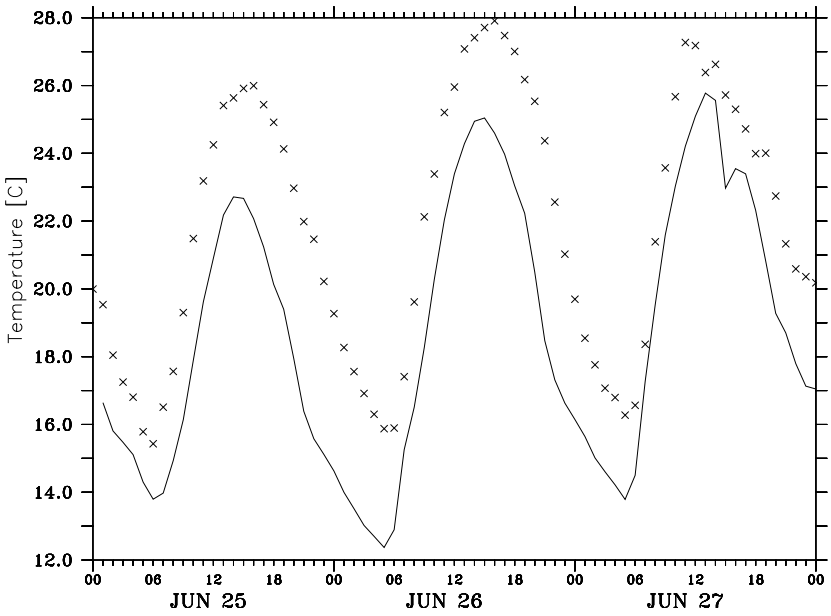

Figure 22: Temperature at 2mAGL in urban areas for a the period June 25 to 27, measured (crosses) and computed by COSMO (solid line) with the operational configuration.

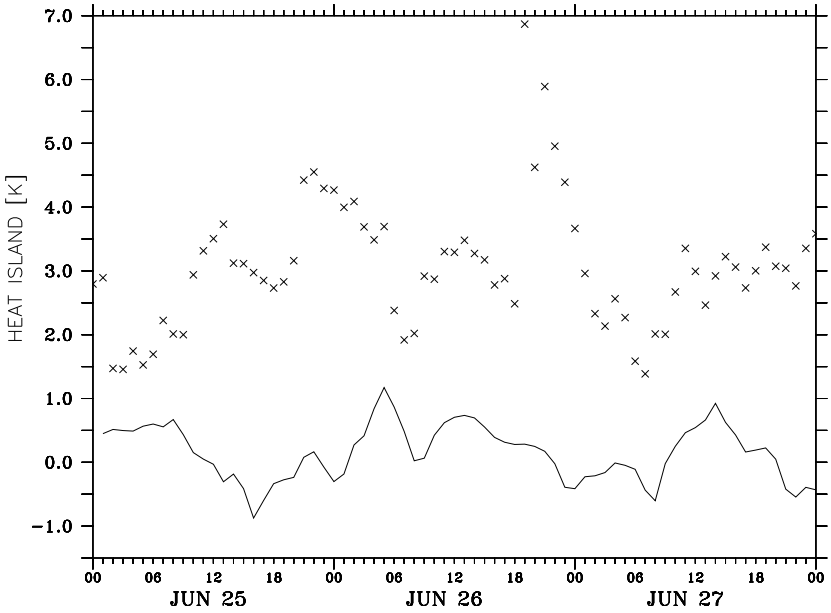

Figure 23: The Urban Heat Island (UHI) at 2mAGL for a three day period (June 25 to 27) measured (crosses) and computed by COSMO (solid line) with the operational configuration.

the boundary layer structure is of crucial importance in order to capture the physics leading to the UHI development.

6.4.1 Increasing The Horizontal Resolution

In order to investigate if the model is able to reproduce the UHI with an increased horizontal resolution, a simulation with the same model setup, and a finer horizontal grid spacing of 2.2 km is performed. This corresponds to the horizontal resolution of the COSMO2 configuration. As with the 7 km resolution, the 2 mAGL temperature in rural area is in good agreement with the measurements (not shown). For urban areas, the temperature is still too low and the UHI is not reproduced (Fig. 24). The average UHI is with 0.1 °C even lower than with a 7 km horizontal resolution. In this case, increasing the horizontal resolution of COSMO has no positive influence on the UHI simulation.

6.4.2 Increasing The Vertical Resolution

In this section, the vertical resolution is increased, applying heights of 20, 26 and 31 m respectively to the first three model layers. The horizontal resolution is kept at 2.2 km, this configuration corresponding to the model setups of COSMO2. As for the simulations with a lower vertical and horizontal resolution, COSMO is not able to reproduce an UHI (Fig. 25). As a conclusion, the ground surface temperature computed by the soil model TERRA_LM and use of the MOST land-surface scheme does not allow to take into account the modifications of the Planetary Boundary Layer (PBL) flow fields induced by the presence of a city. The street canyon geometry reduces sky view factor and wind speed and increases surface area and multiple reflection. Moreover, buildings characteristics modify the energy budget in the city. These factors affect the exchange surfaces-atmosphere from sensible heat and trapping radiation, and cannot be neglected (Oke, 1987). It is necessary to use an adapted parametrization in order to take into account the presence and the effect of a city in the model. For that purpose, the Building Effects Parametrization (BEP), developed by

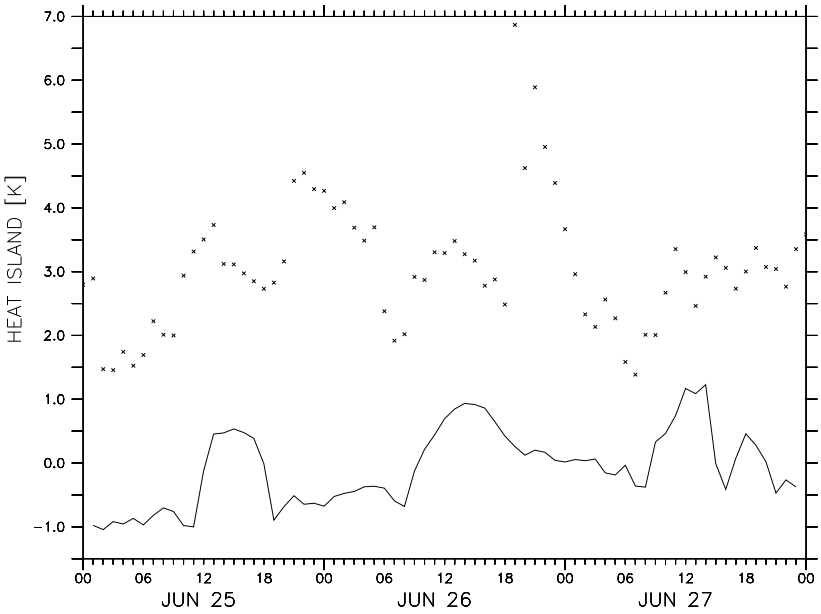

Figure 24: The Urban Heat Island (UHI) at 2m for a three day period (June 25 to 27) measured (crosses) and computed by COSMO (solid line) with an increasing horizontal resolution of 2.2 km.

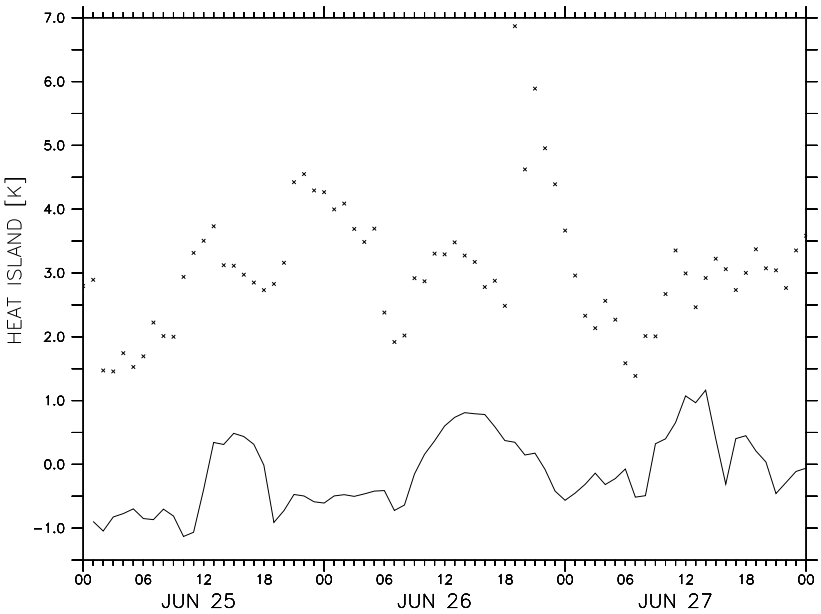

Figure 25: Urban Heat Island (UHI) at 2mAGL for 25 to 27 June, measured (crosses) and computed by COSMO (solid line) with the COSMO2 configuration.

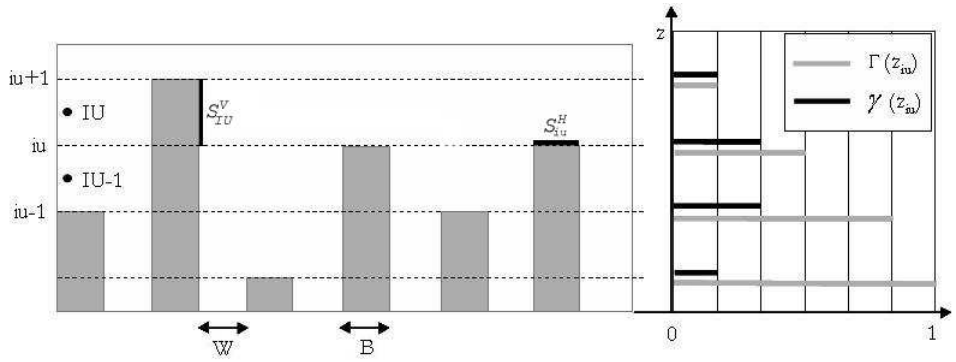

Figure 26: Schematic representation of the city in the urban grid of BEP and the buildings vertical distribution of density $\Gamma(z)$ and probability $\gamma(z)$ (Martilli, 2001).

Martilli et al. (2002) is implemented into the COSMO model.

6.5 BEP : *Building Effects Parametrization*

Results from the last section indicate that there is a clear need to better represent the physical processes of typical urban environments in order to improve the representation of these regions in mesoscale models. In this study we will use the parametrization developed by Martilli (2001) called the Building Effects Parametrization (BEP). It has initially been developed for the mesoscale model FVM and tested extensively on several situation (Martilli, 2002; Roulet et al., 2005) and applied to different cities (Athens (Martilli et al., 2003), Basel (Roulet, 2004), Bogota (Zrate et al., 2006) and Mexico (present work)). This section contains a description of BEP. The next two sections present the implementation of BEP in COSMO and the tests over the city of Basel. BEP takes into account the main characteristics of the urban environment: *(i)* vertical and horizontal surfaces (wall, canyon floor and roofs), *(ii)* shadowing and radiative trapping effects of the buildings, *(iii)* anthropogenic heat fluxes through the buildings wall and roof. In this parametrization the city is represented as a combination of several urban classes. Each class is characterized by an array of buildings (Fig. 26) of the same width B located at the same distance from each other W (canyon width), but with different heights (with a probability $\gamma(z)$ to have a building with height z and a density function $\Gamma(z)$ of buildings with height z or higher). To simplify the formulation we assume that the length of the street canyons is equal to the horizontal grid size. BEP computes urban effects on its own grid. The horizontal resolution is identical to the resolution of the mesoscale grid, while the vertical resolution is generally finer than the mesoscale resolution, and is usually set to 5 meters. Vertically the BEP grid extends up to one layer above the highest buildings. In this parametrization, the fluxes contributions of every urban surface type (canyon floor, roofs and walls) on the momentum, heat and turbulent kinetic energy (TKE) equations are computed separately. Firstly, the contributions of the horizontal surfaces (canyon floor and roofs) are calculated using the formulation of Louis (1979) based on MOST. The roughness lengths used for this calculation are representative for the local roughness of the specific surface types (roofs or canyon floor). Secondly, the exchange of momentum and TKE on the vertical surfaces (walls) are parametrized as the effect of pressure and drag forces induced by the buildings. The temperature fluxes from the walls are a function of the difference between air and wall temperature. They are parametrized using the formulation of Clark (1985) proposed by Arnfield and Grimmond (1998) in their urban energy budget model. The energy budget is computed for every mentioned surface (canyon floor, roofs and walls). Firstly, the direct and infrared radiation at the surfaces are calculated

to take into account the shadowing and radiative trapping effects of the buildings. Then, the surface temperatures for roofs, walls and canyon floor are solved by heat diffusion equation in several layers within the material (concrete or asphalt). After their calculation in the urban grid, the fluxes are vertically interpolated into the mesoscale grid. We will now consider the input parameters that are needed by BEP for each urban class:

Thermal parameters The material thermal diffusivity K_s $[m^2 s^{-1}]$ and specific heat C_s $[Jm^{-3}K^{-1}]$ for each urban surface (roof, canyon floor and wall), as well as building inside temperature T_{int} $[K]$.

Radiation parameters The surface albedo α and emissivity ε for each urban surface (roof, canyon floor and wall).

Roughness parameter The roughness length z_0 $[m]$ for the horizontal surfaces (roof and canyon floor).

Geometrical parameters The street direction, length and width, the buildings height and width, as well as the probability $\gamma(h)$ to have buildings of height h.

Meteorological variables The wind components (u and v), temperature and solar radiation (angle and intensity) from the mesoscale models.

Urban fraction parameter $u_{fraction}(i, j, iurb) \in [0 : 1]$ gives the urban fraction in each cell covering the city.

BEP is then able to compute new surface temperature, momentum, heat and TKE fluxes for each layer of the mesoscale grid influenced by the city.

6.5.1 Temperature at 2 mAGL

The temperatures available for model validation are generally measured at 2 m above the ground. So the model needs to compute the temperature at this height. In COSMO, it is computed as a prognostic variable using MOST, which is based on constant-flux layer approximation in the surface layer. Rotach (1993a,b) shows that the turbulent fluxes are not constant with height in the urban roughness sublayer (1-3 time mean building height) and that similarity theory cannot therefore be applied. As BEP takes into account the presence of a city, its computed fluxes can be used to specify the temperature at 2 m height. For that purpose modifications are implemented in BEP, that will allow to compute diagnostic variables (typically 2 m temperature, 10 m wind) consistent with the land-surface scheme assumptions. The temperature at 2 mAGL corresponds to the temperature simulated in the urban grid, in so far as the first layer near the ground remains thin enough for being considered as the temperature at 2 m. The energy budget equations for sensible heat, momentum and TKE are hence solved in the urban grid. With low horizontal resolution (here 2 km) compared to the high vertical resolution (5 m), vertical fluxes dominate the horizontal fluxes and represent the main source term in the energy budget equation. Therefore the horizontal fluxes can be neglected as shown by Masson et al. (2002) with measurements. The vertical turbulent exchanges balance the fluxes coming from the buildings and the ground, thus the equations for sensible heat, momentum and TKE are parametrized for each layer in the urban grid as follows:

$$\frac{\partial}{\partial z}\left(K_z \frac{\partial \theta}{\partial z}\right) = a_\theta \theta + b_\theta \tag{7}$$

$$\frac{\partial}{\partial z}\left(K_z \frac{\partial U_i}{\partial z}\right) = a_{U_i} U_i + b_{U_i} \tag{8}$$

$$\frac{\partial}{\partial z}\left(K_z \frac{\partial E}{\partial z}\right) = a_E E + b_E + \rho K_z \left[\left(\frac{\partial U_x}{\partial z}\right)^2 + \left(\frac{\partial U_y}{\partial z}\right)^2\right] - \frac{g}{\theta_0}\rho K_z \frac{\partial \theta}{\partial z} - \rho C_\varepsilon \frac{E^{3/2}}{l_\varepsilon} \tag{9}$$

Equations 7 and 8 parametrize respectively the temperature θ and the wind speed U_i for each direction in accordance with Pielke (1984). a_ψ and b_ψ are the flux source terms computed by BEP and K_z $[\frac{m^2}{s}]$ are the vertical diffusion coefficients. Equation 9 $[\frac{m^2}{s^2}]$ is the prognostic equation for the turbulent kinetic energy E according to Bougeault and Lacarrere (1989) with a $k-1$ closure. In this equation, $\rho K_z \left[\left(\frac{\partial U_x}{\partial z}\right)^2 + \left(\frac{\partial U_y}{\partial z}\right)^2\right]$ and $\frac{g}{\theta_0}\rho K_z \frac{\partial \theta}{\partial z}$ are the production terms representing the shear and the buoyancy respectively. The $\rho C_\varepsilon \frac{E^{3/2}}{l_\varepsilon}$ term is the dissipation rate where l_ε is a characteristic length of the energy-containing eddies, and computed as the root square of l_k multiplied by the street width. l_k $[m]$ is a characteristic length for eddies determined as the minimum between street width and height where l_k is computed. C_ε is a numerical coefficient set to 0.71 (Bougeault and Lacarrere, 1989). The system of 4 equations is characterized by 5 unknowns (θ ,U_x, U_y, E and K_z) for each layer of the urban grid. In order to close the system, K_z is defined as a function of E (Bougeault and Lacarrere, 1989) and is written:

$$K_z = C_k l_k E^{1/2}, \tag{10}$$

where C_k is a numerical coefficient set to 0.4 (Bougeault and Lacarrere, 1989).

In BEP, this system is solved by iteration once the flux source terms a_ψ and b_ψ are computed. Firstly TKE is estimated for computing K_z according to equation 10. Then temperature and wind speed are computed with equations 7 and 8, and TKE can be computed with (9). A new K_z is then calculated using the new TKE value, and iterations are made until TKE converge. The energy profile in the urban grid is used to initialize K_z for the next time step. It is necessary to determine the upper-boundary conditions in the urban grid. For wind, they are directly given by the mesoscale models at the height of the urban grid top. For TKE and temperature at the top of the urban grid (above the buildings), it is assumed that a neutral surface layer is developing above the roughness layer (Roth, 2000), which is virtually starting from the zero plane displacement (Oke, 1987) situated in the roughness layer (Fig. 27). In the surface layer, the vertical turbulent fluxes of momentum and heat are assumed to remain constant (Seinfeld and Pandis, 1998). In this case, only the production (shear and buoyancy) and the dissipation terms remain in the prognostic equation for E, *i.e.*

$$\rho C_\varepsilon \frac{E^{3/2}}{l_\varepsilon} = \rho K_z \left[\left(\frac{\partial U_x}{\partial z}\right)^2 + \left(\frac{\partial_U y}{\partial z}\right)^2\right] - \frac{g}{\theta_0}\rho K_z \frac{\partial \theta}{\partial z} \tag{11}$$

In accordance with the assumed surface layer properties, shear is defined as:

$$\rho \frac{U_*^3}{\kappa(z - z_d)}\phi, \tag{12}$$

Where κ is the von Karman constant set to 0.40, under neutral conditions and ϕ is equal to 1 (Businger et al., 1971). U_* is the friction velocity and z_d the zero plan height define as $0.67 * \textit{building height}$ (Grimmond and Oke, 1999). The buoyancy in the surface layer is defined as:

$$\frac{g}{\theta_0}\rho U_* \theta_* \tag{13}$$

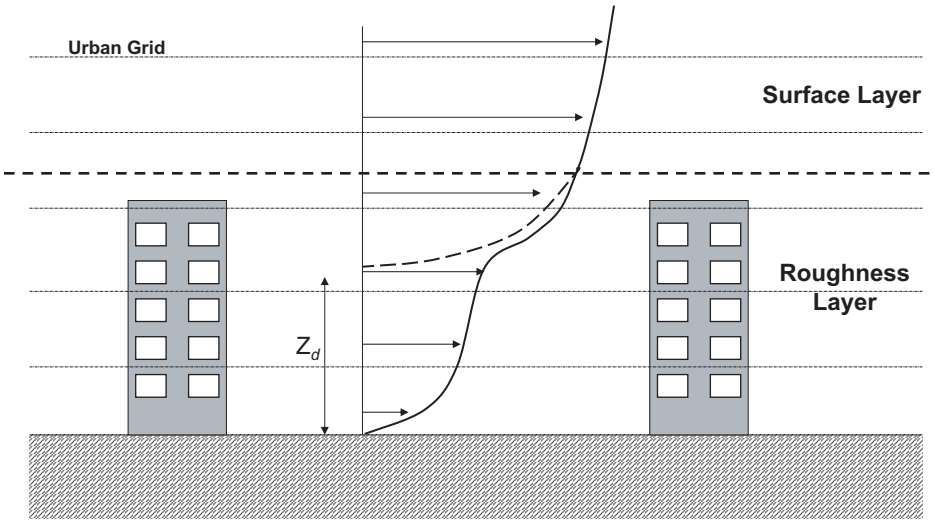

Figure 27: Schematic representation of a wind profile in the roughness layer and in the surface layer. It assumes that a surface layer has developed above the urban canopy and virtually starts at the zero plane displacement height Z_d.

Where θ_* is a potential temperature scale. U_*^2 is the total momentum flux and $U_*\theta_*$ the total heat flux:

$$U_*^2 = \sqrt{(A_{u_x}U_x + B_{u_x})^2 + (A_{u_y}U_y + B_{u_y})^2} \tag{14}$$

$$U_*\theta_* = A_\theta\theta + B_\theta \tag{15}$$

Where A_ψ and B_ψ represent the total source term in the urban grid. Based on (11) and using equations 12 to 15, TKE at the top of the urban grid is estimated as:

$$E_{top} = \left[\frac{1}{C_\varepsilon}\left(\frac{U_*^3}{\kappa} - \frac{g(z-z_d)}{\theta_0}U_*\theta_*\right)\right]^{2/3} \tag{16}$$

The upper-boundary condition for temperature is parametrized with a logarithmic profile (Pielke, 1984),

$$\theta_* = \frac{\kappa(\theta_z - \theta z_d)}{0.74[\ln(z/z_0) - \psi_H(z/L)]} \tag{17}$$

As explained before, the flux θ_* remains constant within the neutral surface layer. A further assumption is to neglect perturbation terms $\psi_H(z/L)$. Temperature $\theta_{z_{top}}$ at the top of the urban grid (z_{top}) can then be expressed as a function of the temperature at the first mesoscale model layer above the urban grid $\theta_{z_{meso}}$:

$$\theta_{z_{top}} = \theta_{z_{meso}} - 0.74\frac{\theta_*}{\kappa}\ln\left(\frac{z_{top}-z_d}{z_{meso}-z_d}\right) \tag{18}$$

The temperature at the urban grid top, $\theta_{z_{top}}$, is linked both to the mesoscale model, by the value above the urban grid $\theta_{z_{meso}}$ and to the urban parametrization, by the potential temperature scale θ_*. This method also solves wind speed and TKE in the urban grid.

6.6 Implementation of BEP in Cosmo

BEP outputs consist of a ground surface temperature and of momentum and heat fluxes profiles calculated over the entire height of the urban grid. In the original version of COSMO, surfaces fluxes are implicitly calculated by the soil module, using the formulations given in equation 6. In the modified version, BEP is implemented in COSMO and runs after the soil module. In the following, two implementation methods are presented.

6.6.1 First Method

The first method is based on the re-computation of the transfer coefficients C_m^d and C_h^d in order to impose surface variable tendencies corresponding to the ones computed in BEP. It is then necessary to find a formulation for the coefficients depending on the tendencies calculated by BEP, (*i.e.* u_{flux}, v_{flux} and t_{flux}). Beginning with the first two equations of system (6):

$$(\tau^{13})_{\zeta=N_\zeta+1/2} = \tau^{13}_{sfc} = -\rho C_m^d |\vec{v}_h| u = -\rho C_m^d \sqrt{u^2+v^2}\, u, \tag{19}$$

$$(\tau^{23})_{\zeta=N_\zeta+1/2} = \tau^{23}_{sfc} = -\rho C_m^d |\vec{v}_h| v = -\rho C_m^d \sqrt{u^2+v^2}\, v, \tag{20}$$

and introducing two new coefficients $C^d_{m,u}$ and $C^d_{m,v}$ to take into account both wind directions u and v:

$$\tau^{13}_{sfc} = -\rho C^d_{m,u} \sqrt{u^2+v^2}\, u, \tag{21}$$

$$\tau^{23}_{sfc} = -\rho C^d_{m,v} \sqrt{u^2+v^2}\, v, \tag{22}$$

with units $[\frac{kg}{ms^2}]$.

BEP module gives the tendencies u_{flux} and v_{flux} with units $[\frac{m}{s^2}]$, coming from wind speed temporal derivative, *i.e.* $\frac{\partial}{\partial t}[\frac{m}{s}]$. Thus, it is possible to find a relation between the tendencies of BEP and the surface fluxes of COSMO. In the following, this relation is derivated for the u-direction:

$$\tau^{13} = \Delta z \rho u_{flux}, \tag{23}$$

where Δz is the height of the first mesoscale layer and ρ is the density. Replacing τ^{13} by (21) and simplifying the density terms, we have:

$$-C^d_{m,u} \sqrt{u^2+v^2}\, u = \Delta z u_{flux}, \tag{24}$$

Finally, resolving for $C^d_{m,u}$ and similarly for the v-direction, we obtain the equations linking the momentum transfer coefficients with the fluxes within BEP:

$$C^d_{m,u,BEP} = -\Delta z \frac{u_{flux}}{u\sqrt{u^2+v^2}},$$

$$C^d_{m,v,BEP} = -\Delta z \frac{v_{flux}}{v\sqrt{u^2+v^2}}, \tag{25}$$

Following a similar approach, we can find a relation between the transfer coefficient C_h^d and the heat flux tendency t_{flux}, with units $[\frac{K}{s}]$. The third equation of (6) becomes:

$$(\hat{H}^3)_{\zeta=N_\zeta+1/2} = \hat{H}^3_{sfc} = -\rho C_h^d |\vec{v}_h| (\theta \pi_{sfc} - T_{sfc})$$

$$= \rho C_h^d \sqrt{u^2+v^2} (T_{sfc} - T_{\zeta=N_\zeta}), \tag{26}$$

with units $[\frac{kgK}{sm^2}]$. We have then to divide $\hat{H}^3_{sfc}$ by a density term ρ and a length term Δz to obtain $[\frac{K}{s}]$. Thus:

$$t_{flux} = \frac{\hat{H}^3_{sfc}}{\rho \Delta z} = \frac{\rho C_h^d \sqrt{u^2+v^2}(T_{sfc} - T_{\zeta=N_\zeta})}{\rho \Delta z}, \tag{27}$$

Again, simplifying the density terms and resolving for C_h^d, lead to an expression linking the transfer coefficient for sensible heat with the tendency given by BEP:

$$C^d_{h,BEP} = \Delta z \frac{t_{flux}}{\sqrt{u^2+v^2}(T_{sfc} - T_{\zeta=N_\zeta})}, \tag{28}$$

These three coefficients calculated by BEP are then used to create the final coefficients for input into COSMO, following a linear combination between BEP's and COSMO's coefficients:

$$\begin{aligned} C^d_{m,i,final} &= u_{fraction} C^d_{m,i,BEP} + (1 - u_{fraction}) C^d_{m,LM}, \\ C^d_{h,sensible,final} &= u_{fraction} C^d_{h,BEP} + (1 - u_{fraction}) C^d_{h,LM}, \end{aligned} \tag{29}$$

where $i = u, v$ and $u_{fraction} \in [0 : 1]$ defines the urban fraction in a mesoscale cell and depends on the landuse type.

We have now to consider the fact that BEP consider urban areas as a set of totally dry surfaces. Thus, the module does not calculate any tendencies for latent heat fluxes. A final coefficient for the latent heat is nevertheless calculated, using the following combination:

$$C^d_{h,latent,final} = (1 - u_{fraction}) C^d_{h,LM}, \tag{30}$$

so that the moisture exchanges at the surface are characterized by the rural fraction $(1 - u_{fraction})$ affected to each urban cell.

As already mentioned, BEP also calculates a street surface temperature tgs_u. The module is defined with three soil layers, the deepest having a constant temperature. At time $t = t_0$, the constant temperature of COSMO is used to initialize the temperature in every soil layers of BEP. Then, the module calculate a thermal gradient over all layers at each time step and gives tgs_u. As for (29) and (30), the final ground surface temperature is calculated with a linear combination between tgs_u from BEP and t_s from COSMO:

$$t\_s_{final} = u_{fraction} tgs\_u + (1 - u_{fraction}) t\_s \tag{31}$$

This temperature finally replaces COSMO's ground surface temperature t_s at each time step.

The advantage of this implementation method of BEP into COSMO is that it requires no knowledge about the code solver and that the model code does not need to be modified. Nevertheless, it is not optimal for several reasons. With such an implementation, only the first mesoscale layer can be influenced by BEP. This means that it is not possible to consider buildings higher than the first mesoscale level. Moreover, terms 25, 25 and 28 show that for low wind speeds the recomputed exchange coefficient may numerically diverge. Thus, it is necessary to control and to limit the transfer coefficients for the low wind speed situations. This implementation method has some limits. Therefore a second method to implement BEP and to take into account the source flux terms above the first layer of the mesoscale model is presented in the next section.

6.6.2 Second Method

The first method is more complex but does not modify the LM code. This second method is simpler and more powerful but modifications must be applied to the implicit LM solver. To avoid the limitations of the first implementation method, a more direct method is presented that needs less modifications in BEP and LM code and acts on each vertical mesoscale layer influenced by urban areas. It relies on the use of tendencies ψ_{flux} and source terms a_ψ and b_ψ, where $\psi = u, v, t$. BEP calculates the tendency u_{flux} using the source terms, as follows

$$u_{flux} = \rho \Delta z (a_u u + b_u), \tag{32}$$

This can be generalized by:

$$\psi_{flux} = \rho \Delta z (a_\psi \psi + b_\psi), \tag{33}$$

where a_ψ and b_ψ are the implicit and explicit source terms respectively and $\rho\Delta z$ a conversion factor from BEP's tendencies and COSMO's fluxes. Now, if we look at equation (33) in term of temporal derivative, we have:

$$\frac{\psi^{n+1} - \psi^n}{\Delta t} = \rho\Delta z(a_\psi \psi^{n+1} + b_\psi), \tag{34}$$

The step is now to implement the tendencies and the source terms in COSMO through equation (4) for k-level only, which means:

$$B_k \psi_k^{n+1} = D_k(\psi^n, ...), \tag{35}$$

Finally, if we take the implicit and explicit terms of (34) and (35), it is possible, by analogy, to connect BEP to COSMO through the source terms:

$$\begin{aligned} B_k &\longrightarrow B_k - a_\psi, \\ D_k &\longrightarrow D_k + b_\psi \end{aligned} \tag{36}$$

Two valuable methods to implement BEP in COSMO have been presented. The choice of the implementation method depends on the user's knowledge of the mesoscale code and on the possibility to modify it. With some adaptations, but keeping the same implementation philosophy, these two methods allow to implement BEP in numerous mesoscale models. Having the possibility to change the implicit solver of LM, the second method is used in this study, which allows to take into account the urban source terms in each layer of the mesoscale grid influenced by the urban canopy.

6.7 Simulation of the Basel UHI

6.7.1 Model Setup

In this part, we keep the same simulation domain over Basel and its surroundings (cf. section 6.3.3) with the COSMO2 configuration *i.e.*, a 2.2 km horizontal resolution, a first layer thickness of 20 m and a 3 day simulation period from June 25 to 27. The characteristics and the fraction of urban area in each cell is determined from the KABA data base (Fehrenbach, 1999). Two city categories are defined:

- *City center*: high density of buildings (15 m high), narrow street and 80% of urban area[4]. Represented by 7 grid points.
- *Sub-urban areas*: smaller density of small buildings (7 m high) and 60% of urban area. Represented by 17 grid points.

Figure 28 shows the simulated domain with cells considered as urban and sub-urban. The properties for both urban and sub-urban categories are determined according to KABA and Roulet (2004) and are presented in Appendix 6.9.3. For the cells containing urban area, the parameters of the rural part have been changed in order to represent park and green area. The main model input parameters are summarized in Table 4.

[4]It means that 80% of the area of the grid cell fluxes are computed by the urban parametrization (BEP) and the rest is handled by the traditional LM parametrization with values for rural area.

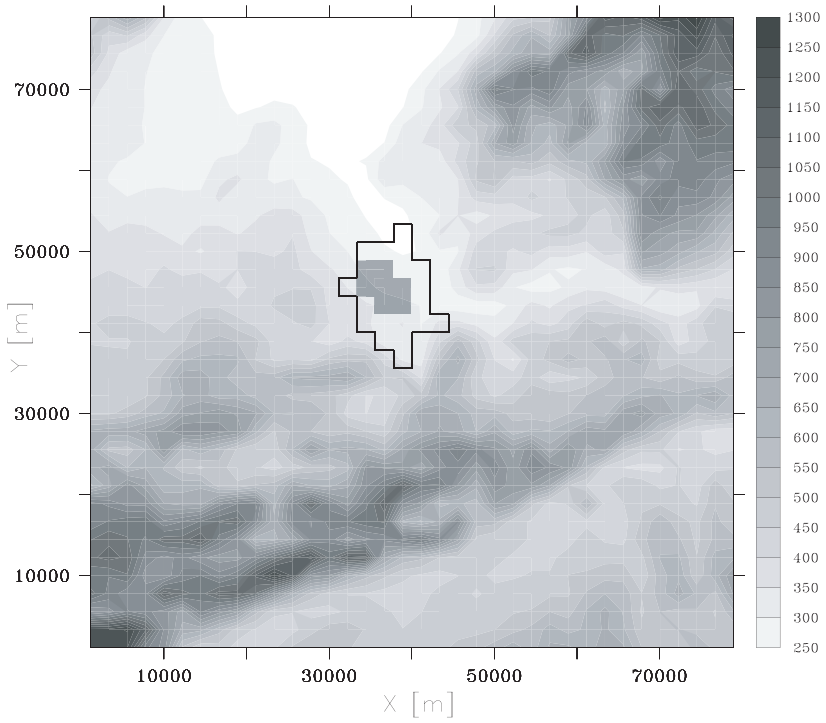

Figure 28: Topography [mASL] of the simulation domain (2.2 km horizontal resolution) over the city of Basel and the urban (gray squares) and sub-urban cells (black shape).

Table 4: The main model input parameters are: nx and ny the number of model grid points in each horizontal direction, nz the number of vertical layers, dx and dy the horizontal grid spacing, dz_{ground} the lowest layer depth and dt the slow modes time step

The main model input parameters	
nx	36
ny	36
nz	60
dx dy	2.2 km
dz_{groud}	20 m
dt	12 min
period	25 to 27 June 2002 (72h)

6.7.2 Results

In this section, we compare results from the mesoscale model calculated both with and without BEP, and give a general overview of the model performance with BEP for the selected episode.

WIND

The wind pattern (Fig. 29 and Fig. 30) is very typical for Basel area with strong inflow from the Rhine valley in the North and going up along the slopes of the terrain. The comparison between simulations with and without BEP shows only slight differences in the wind fields. A small decrease of wind speed over the city is observed with BEP. The air flow simulated without BEP (Fig. 29) is not modified above the city. However, the simulation with BEP (Fig. 30) shows a divergence-convergence system around the city. The simulation shows a divergence and a decrease of the wind speed upstream the city due to drag effect of the buildings. The wind accelerates around the city. Wind speed decreases drastically downstream as a combined effects of drag force and buoyancy due to temperature increase in the city. A convergence is observed south of the city. BEP impacts the air flow up to 7 km upwind and downwind the urban area. Looking hour by hour, we observe that the effect on wind flow increases with wind speed *i.e*, the impact of BEP increases with increasing wind speed.

TEMPERATURE

The simulated temperature at 2 m shows warmer temperature in the urban area with BEP than without. The computed UHI (Fig. 31) is always stronger in the simulations with BEP by 0.7 to 4 °C. The averaged UHI simulated with BEP reaches 2.3 °C, which is in agreement with the measurements (average UHI of 3 °C, Fig. 31). Furthermore, the simulated UHI is late by around 3 hours during the morning and too weak from 18LT to 00LT. We also observed a peak in the measurements at 18 LT on June 26 that the simulation is not able to reproduce. It is instructive to look at absolute temperature values and not differences in order to explain the observed inconsistencies. Figure 32 shows that the city is warmer with BEP particularly during nighttime. The morning temperature increase simulated with BEP comes with a delay, which explains the phase shift of the UHI observed above. Even if the maximum of temperature is too low the first day, it is generally well reproduced with the BEP simulation and the UHI during daytime is well reproduced. The temperature decrease in the afternoon and evening occurs earlier with BEP than in the measurements and a maximum difference between simulation and measurement is reached at sunset (20 LT). This explains the strong UHI anomaly at the end of the day and beginning of the night (cf. Fig. 31). The maximum of measured UHI reached at 18 LT on June 26 is not observed in the urban temperature. This maximum is due to a decrease of the temperature in the rural area (not shown).

Numerous tests have been conducted on the input parameters of BEP used to describe the city. Using typical values found in the literature (Oke, 1987; Masson et al., 2002; Dupont et al., 2004), the following parameters have been varied and sensitivity of the results studied:

- The *Thermal Parameters* of the materials, *i.e.* the thermal diffusivity and the specific heat for roof, wall and ground.
- The *Radiation Parameters* of the surfaces, *i.e.* the albedo and the emissivity of roof, wall and ground.
- The *Roughness Length* of horizontal surfaces (ground and roof).

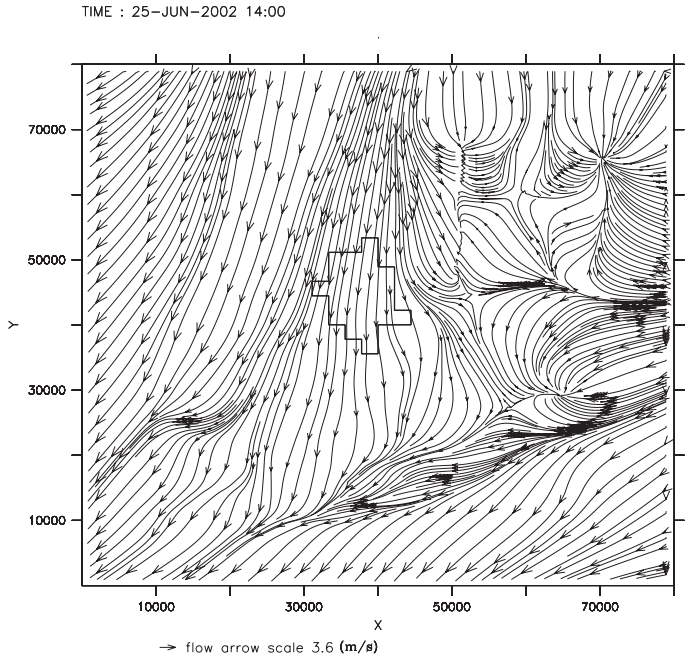

Figure 29: Simulated wind streamline (the size of the arrows indicates the wind speed strength) with COSMO, June 25 at 14LT in the first layer (20 meters height) above and around the city of Basel (black shape).

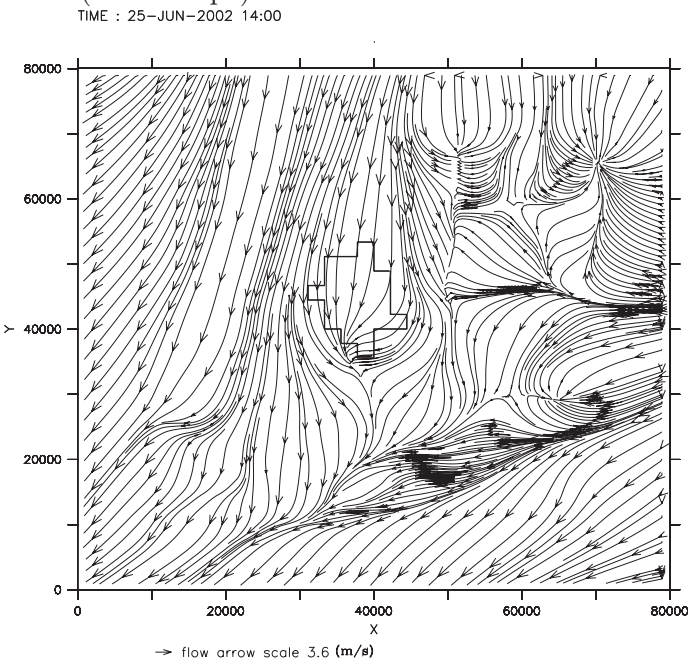

Figure 30: Simulated wind streamline with COSMO/BEP, June 25 at 14LT in the first layer (20 meters height) above and around the city of Basel (black shape).

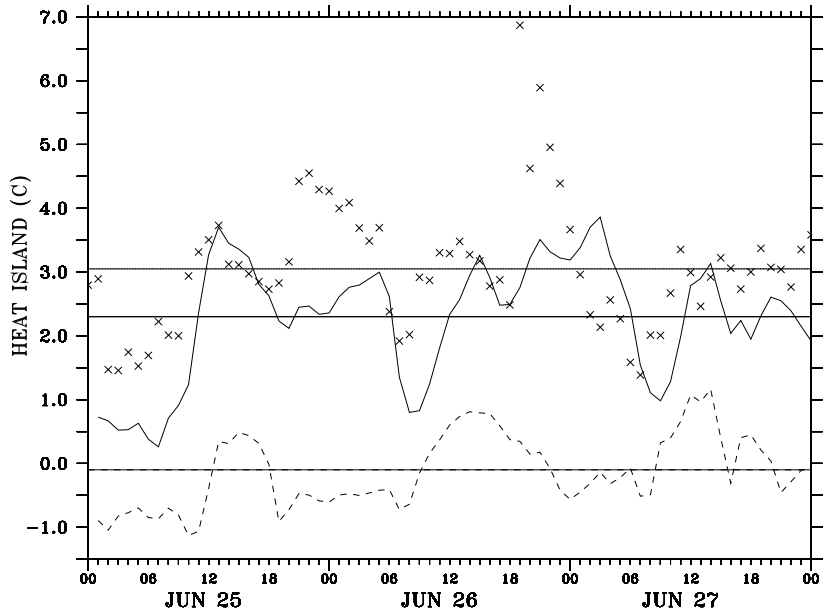

Figure 31: The Urban Heat Island (UHI) at 2m for a three day period (June 25 to 27) measured (crosses) and computed by COSMO with BEP (solid line) and without BEP (dashed line) with an horizontal resolution of 2.2 km

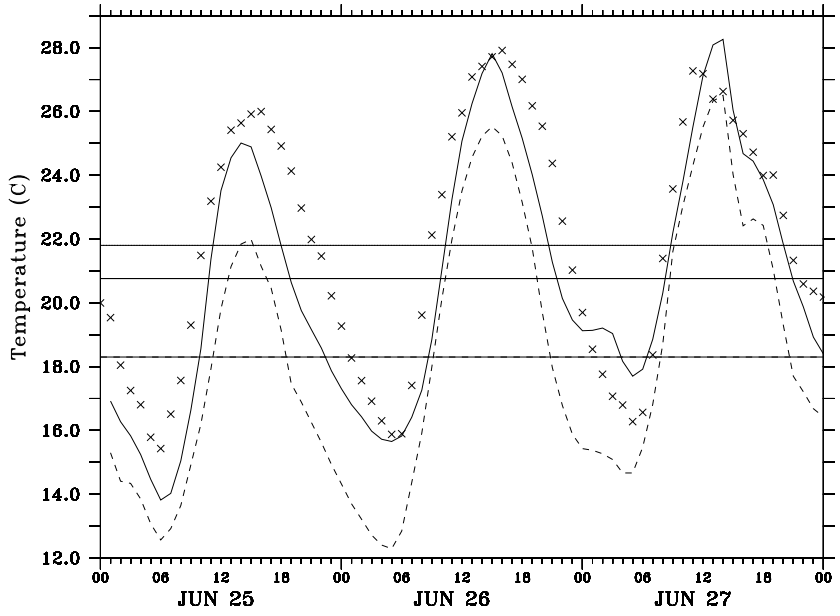

Figure 32: Average temperature at 2 m in the city of Basel, measured (crosses), simulated in COSMO without BEP (dashed line) and with BEP (solid line).

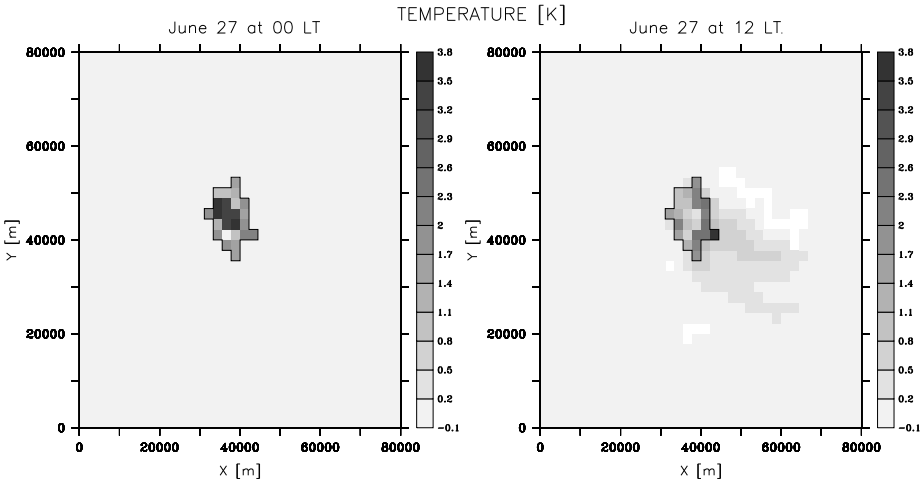

Figure 33: Temperature differences at 2 mAGL [°C] between an COSMO simulation with BEP and without BEP over the city of Basel (black shape) for 27 June, 2002 at midnight (left) and 27 June, 2002 at noon (right)

- The *Geometrical Parameters* of the city, *i.e.* street direction and width, buildings height and width and their repartition.

An impact on the average and on the amplitude of the temperature curve is observed when these parameters are modified. However the shape of the curve is not modified, *i.e.* the morning increase temperature is always late and the temperature decreases too early in the afternoon. Furthermore, modifying the parameters in the range proposed by the literature produces weak impacts (not shown) on the temperature, of around 0.6 °C on the amplitude and 0.3 °C degrees on the average. The results presented above have been computed with the set of parameters that provide the best fit between simulation and measurements. To summarize, the results show that a parametrization of heat and momentum fluxes over urban areas clearly improve mesoscale simulations using an horizontal resolution of 2.2 km. Results with BEP show a much better representation of the UHI as well as the general temperature evolution over an urban area such as Basel. Remaining differences between measured and simulated urban temperatures are dominated by a phase shift in the morning increase and evening decrease. This effect does not show any sensitivity to changes in BEP's input parameters. If measurements are considered representative of the urban environment, this gives an indication that the processes considered in BEP are not complete and some physical mechanisms determining the temperature are not or not well represented.

UHI DISPERSION

Figure 33 shows the difference of temperature at 2 mAGL between a simulation with and without BEP. Two behaviors are observed:

- During nighttime (left panel of Figure 33), the simulation using BEP is clearly warmer above the city by 3.0 to 3.8 °C for the city center and by 1.5 to 2.0 °C for the sub-urban area. During this period, the wind is weak and temperature increase is observed only in the urban cells.

- During daytime (right panel of Figure 33), temperature increase above the city with BEP is weaker than during nighttime (1.5 to 2.5 °C in the city center), however a maximum of 3.4 °C is reached in the east- and southeast-part of the sub-urban area. The wind is stronger during daytime and blows to south east. It creates a displacement

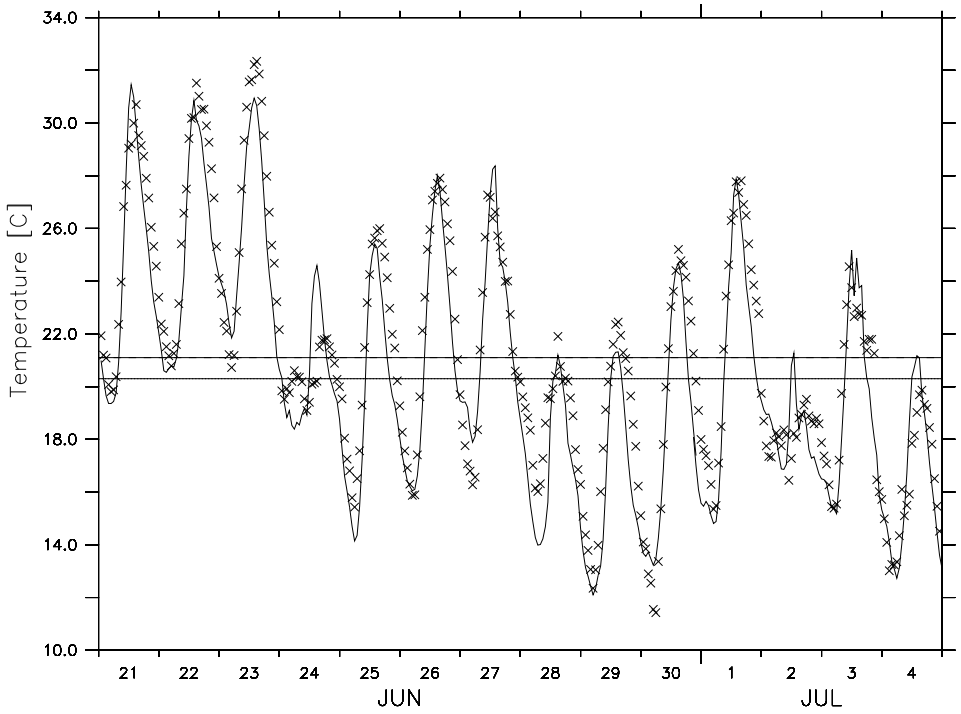

Figure 34: Urban temperature at 2m for a 14 days period (June 21 to July 4, 2002) measured (crosses) and simulated by COSMO with BEP (solid line) with a horizontal resolution of 2.2 km. The horizontal lines are the average of the measured temperature (21.1 °C) and the average of the computed temperature (20.3 °C).

of the maximum and a temperature "plume" which is observed south-east of the city and reaches 0.5 to 1.0 °C.

In both situations BEP increases the temperature in the city. The intensity and diffusion of this temperature increase are strongly dependent on the wind speed, so that BEP modifies not only the urban area but also the nearby area, up to 20 km downwind in the presented case.

6.7.3 14 Days Simulation

Up to now, BEP has only been tested on 2 to 4 day episodes. The implementation of BEP in an operational forecast model gives the opportunity to test it for longer periods (weeks or months) and different kinds of meteorological situations (days with strong cloudiness and/or precipitation). In this section we present a 14 days simulation during the BUBBLE IOP from June 21 to July 4 2002. Figure 34 shows the temperature simulated with COSMO/BEP in the urban area. No tendency being observed, BEP does not accumulate or lose heat during this 14 days period. Thus, BEP is able to compute the urban heat and momentum fluxes for longer period than 3 days. The mean temperature reaches 21.1 °C for measurements, 20.3 °C for the simulation with BEP and 18.3 °C for the simulation without BEP (not shown). The mean temperature is well reproduced with BEP as well as the general temperature behavior. The same tendencies are observed than during the 3 day simulations, which showed a warmer city by 2.4 °C with BEP. During nighttime of 23, 27 and 30 June, BEP slightly overestimates the temperature. The average of the computed UHI (Fig. 35) is 1.6 °C whereas it is around 2.8 °C in the measurements. The difference between measurements and simulation for the UHI is larger than the difference in the urban area temperature

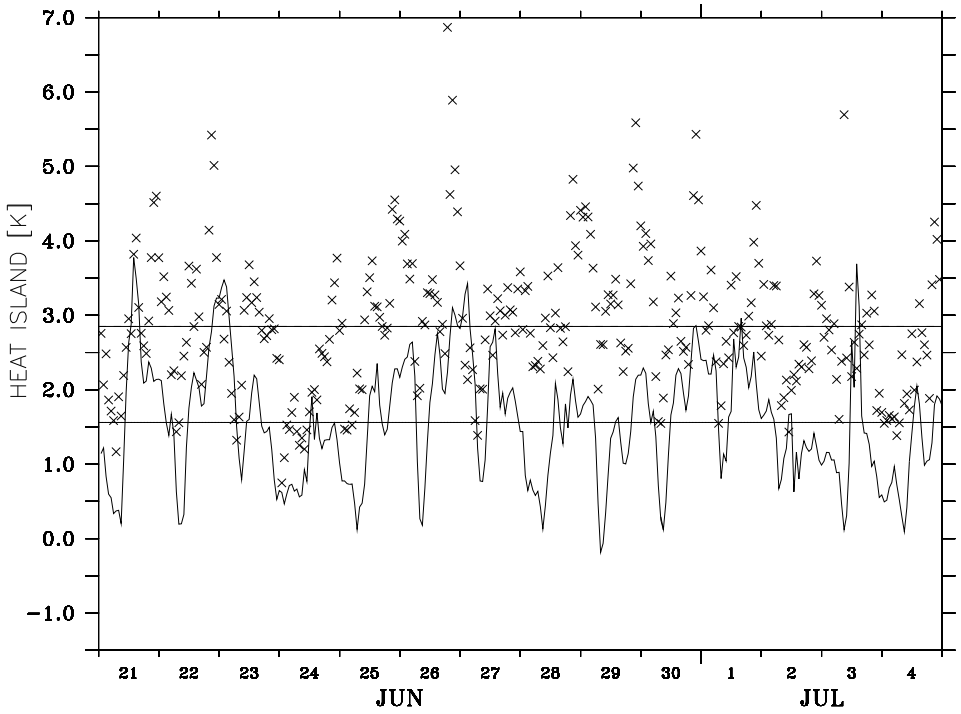

Figure 35: Urban Heat Island (UHI) at 2m for a 14 days period (June 21 to July 4, 2002) measured (crosses) and computed by COSMO with BEP (solid line) with a horizontal resolution of 2.2 km. The horizontal line are the average of the measured and of the computed UHI.

because, in the average, COSMO overestimates the temperature in rural area by 0.4 °C. If we focus on the temperature at 2 mAGL on June 24 when an important rainfall episode occurs form 01LT to 12 LT (Appendix 6.9.2), we observe that the simulation underestimates the temperature during nighttime and overestimates it during daytime. This phenomenon is also observed in the simulation without BEP (not shown), and is probably due to a too weak cloud cover in the simulation. The ground loses too much energy during nighttime by radiative effects and receives too much energy due to incoming solar radiation during daytime. The same phenomenon is observed on July 2 while very weak rainfall is observed during nighttime. However important rainfalls are observed during nighttime from 3 to 4 July and the simulation during this period fits very well to the measurement (Fig. 34). Even if BEP does not take into account latent heat flux, water storage or urban rainfall runoff, the rainfall episode does not deteriorate the results of temperature simulation. Nevertheless, taking into account water budget and latent heat flux in BEP could improve the urban energy balance and the temperature simulation which have shown a too fast cooling at the end of the day (section 6.7.2).

6.8 Conclusion

The presence of a city modifies the fluxes between the atmosphere and the Earth's surface. From August 2001 to July 2002, a year-long measurement campaign (BUBBLE) has been conducted in the city of Basel (Switzerland) and its surroundings with the aim of investigating in details the boundary layer structure in an urban area. During the intensive observation period (IOP), form June 15 to July 12 2002, an Urban Heat Island (UHI) has been underlined by temperature measurements at 2 mAGL inside and outside the city (Table 5). In order to investigate the ability of mesoscale models to take into account the effect of urban areas

Table 5: Average Urban Heat Island (UHI) in °C for the period of June 25 at 00 LT to June 27 at 23LT, for the BUBBLE measurements (left column), an COSMO simulation with 2.2 km horizontal resolution and 20 m vertical resolution for the first layer (center column) and an COSMO simulation and the urban parametrization BEP with the same configuration (right column).

UHI average for June 25 to 27 2002		
Measurement	COSMO	COSMO - BEP
3.0 °C	-0.1 °C	2.3 °C

on atmospheric flow fields and to reproduce the UHI, we have selected a three day episode during the IOP for simulation with the COSMO mesoscale model. COSMO is the operational numerical weather prediction model of MeteoSwiss. It is used on a domain covering most of western Europe with a horizontal resolution of 7 km and a vertical resolution with a 60 m depth for the first layer above the ground. The results obtained with COSMO over the city of Basel and its surroundings shows no UHI. With a 7 km horizontal resolution and a 60 m vertical resolution, the city of Basel and the urban boundary layer are not represented with enough accuracy. In order to investigate if a better resolution allows COSMO to reproduce the measured UHI over Basel, the horizontal resolution has been increased to 2.2 km and the vertical resolution to 20 m for the first layer. The results show that a finer resolution has no impact on the UHI simulation by COSMO (Table 5). As a conclusion, the surface scheme in COSMO based on the similarity theory is not adapted to the urban areas. In order to take into account the presence of a city with a more accurate surface scheme, the Buildings Effects Parametrization (BEP) has been implemented in COSMO. BEP has been modified in order to compute the temperature at 2 mAGL inside the urban canopy. Results show that the implementation is successful and works as expected. The results obtained with BEP show that the urban parametrization modifies the wind flow above and around the city. The wind speed decreases above the city and a system of divergence-convergence is observed around it. Wind divergence-convergence systems are particularly important in air pollution study as they generally lead to a pollution maximum. The temperature is reproduced with a good accuracy in the urban area. Thus, COSMO with BEP is able to reproduce an UHI in the city of Basel (Tab. 5). We have underlined that the temperature increase does not stay confined in the urban area, but extends around the city up to 15 to 20 km. Nevertheless, the UHI computed with BEP is generally too weak (Tab. 5) and even with tuning the urban parameters, BEP is not able to reach the measured values. Sometime, a phase shift is also observed between the measured and simulated temperature. BEP is based on a simplified representation of the urban area and several phenomenon are neglected. The urban parametrization could be adapted in order to take into account different phenomenon, which should modify the urban energy balance:

- The vertical surfaces in BEP are uniform and opaque. Take into account the **windows** will modifying the radiative budget at wall surfaces and in the buildings.
- The **temperature inside the buildings** is maintained constant during the simulation. It will be necessary to take into account its variations in order to represent the buildings energy budget more realistically.
- The **natural ventilation** is the air exchange between inside and outside the buildings (windows opened, ventilation, ...). Koutrakis et al. (1992) estimated that more than 50% of the buildings volume of air can directly be exchanged with the outdoor each

hour.

- The **air conditioning** cools down the air inside and rejects heat in the urban atmosphere. It modifies the balance between inside and outside buildings, and is an important source of heat due to its energy consumption.
- No **urban water budget** is computed in BEP. It doesn't take into account precipitation, pipped water supply of the city and water vapor released due to anthropogenic activities, such as combustion.

A 14 days period has been simulated with COSMO/BEP. It is the first time that BEP is applied for a such long period. That allows to verify that BEP does not accumulate or lose energy and that it can be used for long term simulations. Rainfall episodes are included in these 14 days. BEP does not take into account latent heat flux, water storage and urban rainfall runoff. Nevertheless, the simulation with BEP are in good agreement with the measurements. The results show the importance to have an adapted parametrization for urban areas in order to take into account the modification of the atmospheric flow fields induced by the presence of a city. The increase of horizontal and vertical resolution in COSMO2 is not sufficient to take into account the presence of a city, the use of an adapted parametrization is necessary. BEP implementation in COSMO is a distinct enhancement for the simulation above urbanized region. We have focused our study on the 2 m observations for temperature, 10 m observations for the wind and the horizontal dispersion of the UHI. The urban effects are also present in the vertical direction. It is important to investigate the impact of BEP on the vertical structure of the atmosphere and its capacity to be used with a low resolution mesoscale model for operational forecast purposes.

References

Arnfield, A. J. and Grimmond, C. S. B., 1998. An Urban Canyon Energy Budget Model and its Application to Urban Storage Heat Flux Modelling, *Energ. Buildings*, **27**, 61–68.

Bougeault, P. and Lacarrere, P., 1989. Parameterisation of Orography-Induced Turbulence in a Mesobeta-Scale Model, *Mon. Wea. Rev.*, **117**, 1872–1890.

BUBBLE. *http://pages.unibas.ch/geo/mcr/Projects/BUBBLE.*

Businger, J. A., Wyngaard, J. C., Izumi, Y., Bradley, E. F., 1971. Flux-Profile Relationships in the Atmospheric Surface Layer, *J. Atmos. Sci.*, **28**, 181–189.

Clarke, J. A., 1985. *Energy Simulation in Building Design*, Adam Hilger, Bristol, 362 pp.

COSMO. *http://www.cosmo-model.org/public/documentation.htm.*

Doms, G., Fäurstner, J., Heise, E., Herzog, H.-J., Raschendorfer, M., Schrodin, R., Reinhardt, T., Vogel, G., 2002. A Description of the Nonhydrostatic Regional Model LM, Part I: Dynamics and Numerics, *Documentation of the LM Package*, 2nd version.

Doms, G., Fäurstner, J., Heise, E., Herzog, H.-J., Raschendorfer, M., Schrodin, R.,Reinhardt, T., Vogel, G., 2002. A Description of the Nonhydrostatic Regional Model LM, Part II: Physical Parameterization, *Documentation of the LM Package*, 2nd version.

Dupont, S., Otte, T.L. and Ching, J.K.S., 2004. Simulation of meteorological fields within and above urban and rural canopies with a mesoscale model, *Boundary-Layer Meteorol.*, **113** (1), 11–158.

Fehrenbach, U., 1999. Analyse und Bewertung lokal- und regional-klimatisch wirksamer Faktoren in der Region Basel, Diss. Phil.-Nat. Fak., Univ. Basel, ISBN 3-85977-245-7.

Grimmond, C. S. B., Oke, T. R., 1999. Aerodynamic Properties of Urban Areas Derived from Analysis of Surface Form, *J. Appl. Meteorol.*, **38**, 1262–1292.

Koutrakis, P., Briggs, S.L.K., Leaderer, B. P., 1992. Source Apportionment of Indoor Aerosols in Suffolk and Onondag Counties, New York, *Environ. Sci. Technol.*, **26**, 521–527.

Hamdi, R., 2005. Validation for the cities of Basel and Marseilles, *PhD Thesis*. Université catholique de Louvain, Belgium.

Louis, J.-F., 1979. A parametric model of vertical eddy fluxes in the atmosphere, *Bound.-Layer Meteor.*, **17**, 187–202.

Martilli, A., 2001. Development of an urban turbulence parameterisation for mesoscale atmospheric models, *PhD Thesis N^o* **2445**. Federal Institute of Technology (EPFL), Lausanne, Switzerland.

Martilli, A., Clappier, A., Rotach, M. W., 2002. An urban surfaces exchange parameterisation for mesoscale models, *Bound.-Layer Meteor.*, **104**, 261–304.

Martilli, A., 2002. Numerical study of urban impact on the boundary layer structure: sensitivity to wind speed and urban morphology, and rural soil moisture, *J. Appl. Meteorol.*, **41**, 1247–1267.

Martilli, A., Roulet, Y.-A., Junier, J., Kirchner, F., Rotach, M. W., Clappier, A., 2003. On the impact of urban surface exchange parameterisations on air quality simulations: the Athens case, *Atmos. Environ.*, **37**, 4217–4231.

Masson, V., 2000. A Physically-Based Scheme For The Urban Energy Budget In Atmospheric Models, *Bound.-Layer Meteor*, **94**, 357–397.

Masson, V., Grimmond, C.S.B, Oke, T.R., 2002. Evaluation of the Town Energy Balance (TEB) scheme with direct measurements from dry districts in two cities, *J. Applied Meteorol.*, **41**, 1011–1026.

Oke, T.R, 1987. Boundary Layer Climates, 2nd edn. London: Methuen, 435 pp.

Orlanski, L., 1975. A rational subdivision of scales for atmospheric processes, *Bull. Amer. Meteor. Soc.*, **56**, 527–534.

Pielke, R., 1984. *Mesoscale Meteorological Modeling*, Academic Press, San Diego, pp 612.

Rotach, M. W., 1993. Turbulence close to a rough urban surface. Part I: Reynolds stress, *Bound.-Layer Meteor.*, **65**, 1–28.

Rotach, M. W., 1993. Turbulence close to a rough urban surface Part II: variances and gradients, *Bound.-Layer Meteor.*, **66**, 75–92.

Rotach, M. W., Vogt, R., Bernhofer, C., Batchvarova, E., Christen, A., Clappier, A., Feddersen, B., Gryning, S.-E., Martucci, G., Mayer, H., Mitev, V., Oke, T. R., Parlow, E., Richner, H., Roth, M., Roulet, Y.-A., Ruffieux, D., Salmond, J. A., Schatzmann M., Voogt, J. A., 2005. BUBBLE - an Urban Boundary Layer Meteorology Project, *Theor. Appl. Climatol.*, **81**, 231–261.

Roth, M., 2000. Review of atmospheric turbulence over cities, *Q. J. R. Meteorol. Soc.*, **126**, 941–990.

Roulet, Y.-A., 2004. Validation and Application of an urban turbulence parameterisation scheme for mesoscale atmospheric models, *PhD Thesis N°*. **3032**, Swiss Federal Institute of Technology, Lausanne.

Roulet, Y.-A., Martilli, A., Rotach, M. W., Clappier, A., 2005. Validation of an urban surface exchange parameterization for mesoscale models - 1D case in a street canyon, *J. of App. Meteorol.*, **44**, 1484–1498.

Seinfeld, J. H., Pandis, S. N., 1998. Atmospheric Chemistry and Physics, *Wiley Interscience publication*, New-York, pp 1326.

Stull, R.B., 1988. An Introduction to Boundary Layer Meteorology, Kluwer Academic Publisher, Dordrecht, pp 670.

Zarate, E., Clappier, A., Belalcazar, L. C., 2006. A study of the photochemical plume formed in Bogota (Colombia) using numerical simulations, *submitted to J. Environ. Manage.*

6.9 Appendices

6.9.1 Bubble Measuring Stations

List of the measuring stations available during the BUBBLE IOP. The first letter of the station code correspond to the situation of the station (U for Urban area, S for Sub-Urban area and R for Rural area).

Code on map (Fig. 18)	Station Name	Height [mASL]
Rp6	Aesch Schlatthof	353
Se1	Allschwil	277
Rp7	Airport Basel-Mulhouse	
Sp2	Basel - Bumlihof	289
Sp3	Basel - Binningen (ANETZ, NABEL)	316
Up6	Basel - Feldbergstrasse	255
Ue4	Basel - Horburg	254
Re3	Basel - Lange Erlen	275
Up7	Basel - Leonhard	273
Ue5	Basel - Kleinhningen	265
Up8	Basel - Novartis Klybeck	255
Ue3	Basel - Messe	255
Up9	Basel - Novartis St.Johann	257
Up10	Basel - Roche	255
Ue2	Basel - Spalenring	278
Ue1	Basel- Sperrstrasse	255
Up11	Basel- St. Johann	260
Rp11	St. Chrischonaturm	490
Sp4	Dornach	325
Re4	Gempen	710
Re1	Grenzach	265
Sp5	Liestal LHA	320
Rp8	Oetlingen	450
Rp9	Pratteln Hardwasser	272
Sp6	Rheinfelden	285
Rp10	Schnenbuch	400
Sp7	Schweizerhalle	270
Re5	St. Louis	250
Re2	Village Neuf	240
Sp8	Weil am Rhein	250

6.9.2 Meteorological Situation during the IOP

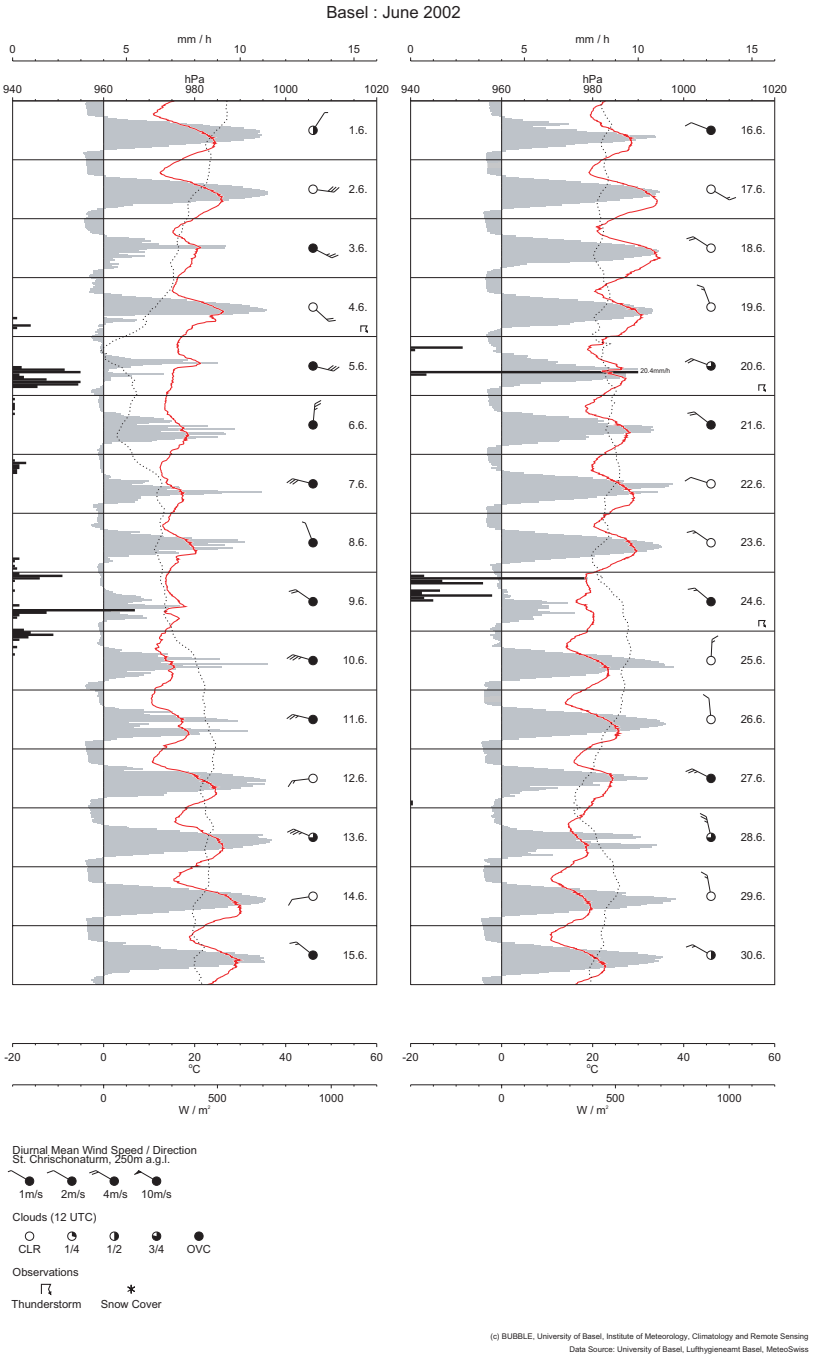

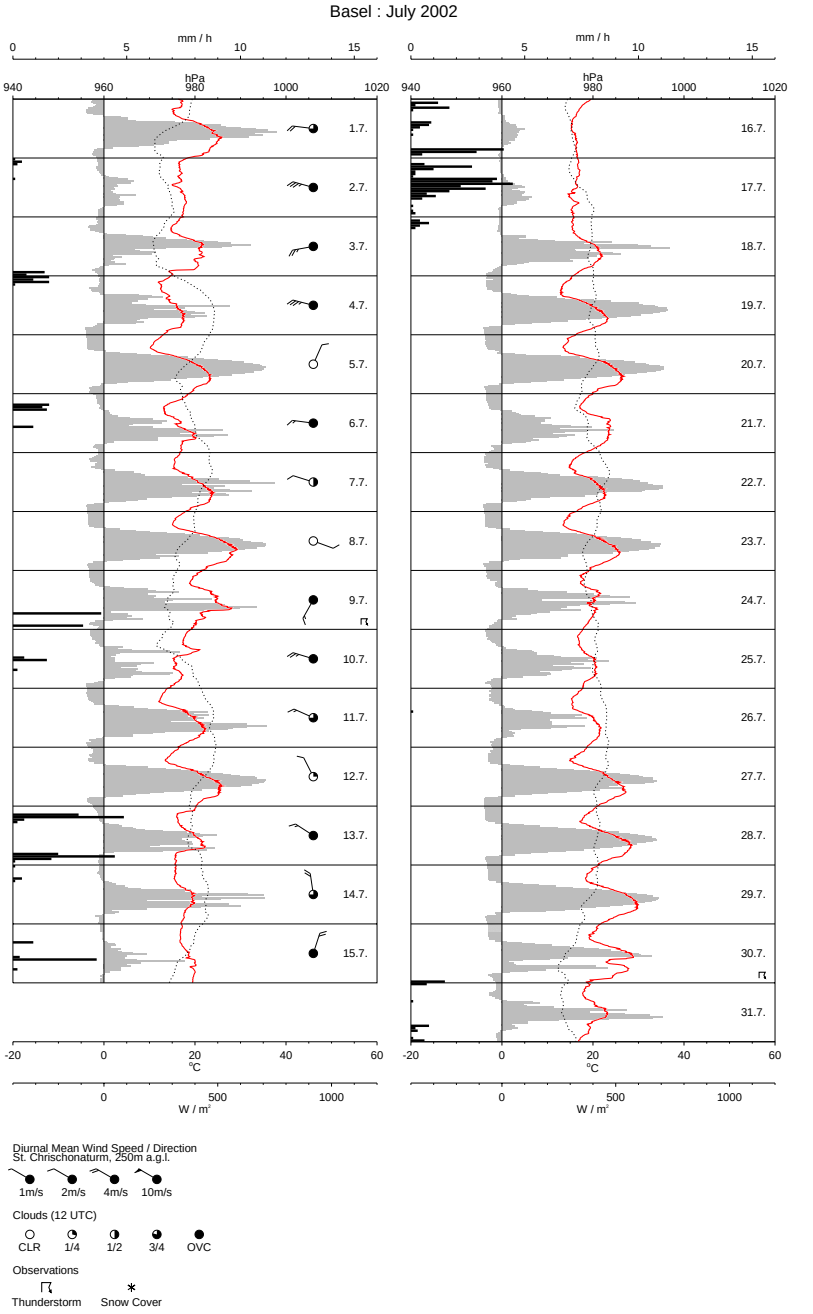
Basel : July 2002
mm / h
hPa
1.7.
2.7.
3.7.
4.7.
5.7.
6.7.
7.7.
8.7.
9.7.
10.7.
11.7.
12.7.
13.7.
14.7.
15.7.
16.7.
17.7.
18.7.
19.7.
20.7.
21.7.
22.7.
23.7.
24.7.
25.7.
26.7.
27.7.
28.7.
29.7.
30.7.
31.7.
°C
W / m²
Diurnal Mean Wind Speed / Direction
St. Chrischonaturm, 250m a.g.l.
1m/s 2m/s 4m/s 10m/s
Clouds (12 UTC)
CLR 1/4 1/2 3/4 OVC
Observations
Thunderstorm
Snow Cover
(c) BUBBLE, University of Basel, Institute of Meteorology, Climatology and Remote Sensing
Data Source: University of Basel, Lufthygieneamt Basel, MeteoSwiss

6.9.3 The Definition of Urban Categories for BEP

The urban properties as they are described in COSMO for the city of Basel

```
URBAN CATEGORY


!     Building parameters
! Ground thermal diffusivity [m^[m^2 s^-1]
      alag_u(1)=0.3e-06,
! Wall thermal diffusivity [m^2 s^-1]
      alaw_u(1)=0.2e-06,
! Roof thermal diffusivity [m^2 s^-1]
      alar_u(1)=0.2e-06,
! Specific heat of the ground material [J m^3 K^-1]
      csg_u(1)=1.4e+6,
! Specific heat of the wall material [J m^3 K^-1]
      csw_u(1)=0.2e+6,
! Specific heat of the roof material [J m^3 K^-1]
      csr_u(1)=0.2e+6,
! Temperature inside the buildings behind the wall [K]
      twini_u(1)=295.,
! Temperature inside the buildings behind the roof [K]
      trini_u(1)=295.,
!     Radiation parameters
! Albedo of the ground
      albg_u(1)=0.2,
! Albedo of the wall
      albw_u(1)=0.2,
! Albedo of the roof
      albr_u(1)=0.2,
! Emissivity of ground
      emg_u(1)=0.95,
! Emissivity of wall
```

```
      emw_u(1)=0.9,
! Emissivity of roof
      emr_u(1)=0.9,
!     Roughness parameters
! The ground's roughness length
      z0g_u(1)=0.0005,
! The roof's roughness length
      z0r_u(1)=0.0005,
!     Street configuration parameters
! Number of street direction
for each urban class
      nd_u(1)=2,
! Street direction [radian]
      drst_u(1,1)=0.7854, !45.*pi/180.
      drst_u(2,1)=2.3562, !135.*pi/180.
! Street width [m]
      ws_u(1,1)=15.,
      ws_u(2,1)=15.,
! Building width [m]
      bs_u(1,1)=22.,
      bs_u(2,1)=22.,
! Bulding's heights [m]
      h_b(1,1)=10.,
      h_b(2,1)=15.,
      h_b(3,1)=17.,
! The probability that a building has an height h_b
      d_b(1,1)=20.,
      d_b(2,1)=55.,
      d_b(3,1)=25.,
```

```
SUB-URBAN CATEGORY


!     Building parameters
! Ground thermal diffusivity [m^2 s^-1]
      alag_u(2)=0.47e-6,
! Wall thermal diffusivity [m^2 s^-1]
      alaw_u(2)=0.37e-06,
! Roof thermal diffusivity [m^2 s^-1]
      alar_u(2)=0.42e-06,
! Specific heat of the ground material [J m^3 K^-1]
      csg_u(2)=1.75e+6,
! Specific heat of the wall material [J m^3 K^-1]
      csw_u(2)=0.5e+6,
! Specific heat of the roof material [J m^3 K^-1]
      csr_u(2)=0.5e+6,
! Temperature inside the buildings behind the wall [K]
      twini_u(2)=293.,
! Temperature inside the buildings behind the roof [K]
      trini_u(2)=293.,
!     Radiation parameters
! Albedo of the ground
      albg_u(2)=0.2,
! Albedo of the wall
      albw_u(2)=0.2,
! Albedo of the roof
      albr_u(2)=0.2,
! Emissivity of ground
      emg_u(2)=0.95,
! Emissivity of wall
      emw_u(2)=0.9,
! Emissivity of roof
      emr_u(2)=0.9,
```

```
!     Roughness parameters
! The ground's roughness length
      z0g_u(2)=0.005,
! The roof's roughness length
      z0r_u(2)=0.005,
!     Street configuration parameters
! Number of street direction
for each urban class
      nd_u(2)=2,
! Street direction [radian]
      drst_u(1,2)=0.7854, !.45.*pi/180.
      drst_u(2,2)=2.3562, !135.*pi/180.
! Street width [m]
      ws_u(1,2)=25.,
      ws_u(2,2)=25.,
! Building width [m]
      bs_u(1,2)=17.,
      bs_u(2,2)=17.,
! Building's heights [m]
      h_b(2,2)=6.,
      h_b(3,2)=9.,
! The probability that a building has an height h_b
      d_b(1,2)=75.,
      d_b(2,2)=25.,
```

7 References

Ament, F. and Simmer, C., 2006. Improved Representation of Land-Surface Heterogeneity in a Non-Hydrostatic Numerical Weather Prediction Model. *Boundary-Layer Meteorology*, **121**, 153–174.

Colbeck, S.C., 1978. The physical aspects of water flow through snow. *Adv. Hydrosci.*, **11**, 165–206.

Heinemann, G. and Kerschgens, M., 2005. Comparison of methods for area-averaging surface energy fluxes over heterogeneous land surfaces using high-resolution non-hydrostatic simulations. *Int. J. Clim.*, **25**, 379–403.

Ritter, B., 2007. Einführung GME-Version 2.13. Änderungsmitteilung operationelles NWV-System, Deutscher Wetterdienst, Offenbach.

List of COSMO Newsletters and Technical Reports

(available for download from the COSMO Website: www.cosmo-model.org)

COSMO Newsletters

No. 1: February 2001.

No. 2: February 2002.

No. 3: February 2003.

No. 4: February 2004.

No. 5: April 2005.

No. 6: July 2006.

No. 7: April 2008; Proceedings from the 8th COSMO General Meeting in Bucharest, 2006.

No. 8: September 2008; Proceedings from the 9th COSMO General Meeting in Athens, 2007.

No. 9: December 2008.

No. 10: March 2010.

No. 11: April 2011.

No. 12: April 2012.

No. 13: April 2013.

No. 14: April 2014.

No. 15: July 2015.

COSMO Technical Reports

No. 1: Dmitrii Mironov and Matthias Raschendorfer (2001):
Evaluation of Empirical Parameters of the New LM Surface-Layer Parameterization Scheme. Results from Numerical Experiments Including the Soil Moisture Analysis.

No. 2: Reinhold Schrodin and Erdmann Heise (2001):
The Multi-Layer Version of the DWD Soil Model TERRA_LM.

No. 3: Günther Doms (2001):
A Scheme for Monotonic Numerical Diffusion in the LM.

No. 4: Hans-Joachim Herzog, Ursula Schubert, Gerd Vogel, Adelheid Fiedler and Roswitha Kirchner (2002):
LLM ¯ the High-Resolving Nonhydrostatic Simulation Model in the DWD-Project LITFASS.
Part I: Modelling Technique and Simulation Method.

No. 5: Jean-Marie Bettems (2002):
EUCOS Impact Study Using the Limited-Area Non-Hydrostatic NWP Model in Operational Use at MeteoSwiss.

No. 6: Heinz-Werner Bitzer and Jürgen Steppeler (2004):
Documentation of the Z-Coordinate Dynamical Core of LM.

No. 7: Hans-Joachim Herzog, Almut Gassmann (2005):
Lorenz- and Charney-Phillips vertical grid experimentation using a compressible nonhydrostatic toy-model relevant to the fast-mode part of the 'Lokal-Modell'.

No. 8: Chiara Marsigli, Andrea Montani, Tiziana Paccagnella, Davide Sacchetti, André Walser, Marco Arpagaus, Thomas Schumann (2005):
Evaluation of the Performance of the COSMO-LEPS System.

No. 9: Erdmann Heise, Bodo Ritter, Reinhold Schrodin (2006):
Operational Implementation of the Multilayer Soil Model.

No. 10: M.D. Tsyrulnikov (2007):
Is the particle filtering approach appropriate for meso-scale data assimilation ?

No. 11: Dmitrii V. Mironov (2008):
Parameterization of Lakes in Numerical Weather Prediction. Description of a Lake Model.

No. 12: Adriano Raspanti (2009):
COSMO Priority Project "VERification System Unified Survey" (VERSUS): Final Report.

No. 13: Chiara Marsigli (2009):
COSMO Priority Project "Short Range Ensemble Prediction System" (SREPS): Final Report.

No. 14: Michael Baldauf (2009):
COSMO Priority Project "Further Developments of the Runge-Kutta Time Integration Scheme" (RK): Final Report.

No. 15: Silke Dierer (2009):
COSMO Priority Project "Tackle deficiencies in quantitative precipitation forecast" (QPF): Final Report.

No. 16: Pierre Eckert (2009):
COSMO Priority Project "INTERP": Final Report.

No. 17: D. Leuenberger, M. Stoll and A. Roches (2010):
Description of some convective indices implemented in the COSMO model.

No. 18: Daniel Leuenberger (2010):
Statistical analysis of high-resolution COSMO Ensemble forecasts in view of Data Assimilation.

No. 19: A. Montani, D. Cesari, C. Marsigli, T. Paccagnella (2010):
Seven years of activity in the field of mesoscale ensemble forecasting by the COSMO–LEPS system: main achievements and open challenges.

No. 20: A. Roches, O. Fuhrer (2012):
Tracer module in the COSMO model.

No. 21: Michael Baldauf (2013):
A new fast-waves solver for the Runge-Kutta dynamical core.

No. 22: C. Marsigli, T. Diomede, A. Montani, T. Paccagnella, P. Louka, F. Gofa, A. Corigliano (2013):
The CONSENS Priority Project.

No. 23: M. Baldauf, O. Fuhrer, M. J. Kurowski, G. de Morsier, M. Müllner, Z. P. Piotrowski, B. Rosa, P. L. Vitagliano, D. Wójcik, M. Ziemiański (2013):
The COSMO Priority Project 'Conservative Dynamical Core' Final Report.

No. 24: A. K. Miltenberger, A. Roches, S. Pfahl, H. Wernli (2014):
Online Trajectory Module in COSMO: a short user guide.

No. 25: P. Khain, I. Carmona, A. Voudouri, E. Avgoustoglou, J.-M. Bettems, F. Grazzini (2015):
The Proof of the Parameters Calibration Method: CALMO Progress Report.

No. 26: D. Mironov, E. Machulskaya, B. Szintai, M. Raschendorfer, V. Perov, M. Chumakov, E. Avgoustoglou (2015):
The COSMO Priority Project 'UTCS' Final Report.

COSMO Technical Reports

Issues of the COSMO Technical Reports series are published by the *COnsortium for Small-scale MOdelling* at non-regular intervals. COSMO is a European group for numerical weather prediction with participating meteorological services from Germany (DWD, AWGeophys), Greece (HNMS), Italy (USAM, ARPA-SIMC, ARPA Piemonte), Switzerland (MeteoSwiss), Poland (IMGW), Romania (NMA) and Russia (RHM). The general goal is to develop, improve and maintain a non-hydrostatic limited area modelling system to be used for both operational and research applications by the members of COSMO. This system is initially based on the COSMO-Model (previously known as LM) of DWD with its corresponding data assimilation system.

The Technical Reports are intended

- for scientific contributions and a documentation of research activities,
- to present and discuss results obtained from the model system,
- to present and discuss verification results and interpretation methods,
- for a documentation of technical changes to the model system,
- to give an overview of new components of the model system.

The purpose of these reports is to communicate results, changes and progress related to the LM model system relatively fast within the COSMO consortium, and also to inform other NWP groups on our current research activities. In this way the discussion on a specific topic can be stimulated at an early stage. In order to publish a report very soon after the completion of the manuscript, we have decided to omit a thorough reviewing procedure and only a rough check is done by the editors and a third reviewer. We apologize for typographical and other errors or inconsistencies which may still be present.

At present, the Technical Reports are available for download from the COSMO web site (www.cosmo-model.org). If required, the member meteorological centres can produce hard-copies by their own for distribution within their service. All members of the consortium will be informed about new issues by email.

For any comments and questions, please contact the editor:

Massimo Milelli
Massimo.Milelli@arpa.piemonte.it